NTNU – Trondheim
Norwegian University of
Science and Technology

Silicon for silicon nitride based products

Harald Øvregård

Materials Science and Engineering
Submission date: June 2013
Supervisor: Mari-Ann Einarsrud, IMTE
Co-supervisor: Kjell Wiik, IMTE
Johan Svanem, Elkem AS Silicon Materials
Harry Rong, Elkem AS Silicon Materials

Norwegian University of Science and Technology
Department of Materials Science and Engineering

Preface

The work of this master thesis has been conducted at the Department of Materials Science and Engineering at the Norwegian University of Science and Technology (NTNU). The work has been done in collaboration with Elkem and carried out during the spring of 2013. This report presents the results from the nitridation of silicon powder after storing in different humid atmospheres.

The master thesis has been carried out independently, honest and in accordance with the examination regulations of NTNU

Trondheim, June 2013

Harald Øvregård

Acknowledgement

First of all, I would like to thank my supervisor professor Mari-Ann Einarsrud for a very good follow up over the last year. She has arranged weekly meetings and discussions and given me very productive feedback. The fact that she always keeps appointments and has encouraged me to come to her for advice has been very helpful for the progress of this work and for that I am very grateful.

A big thanks to M.Sc. Johan Pääaho Svanem from Elkem, who has shown great interest in my work and given me much appreciated feedback in our many meetings. I would also like to thank professor Kjell Wiik for helping me whenever I needed it and for good assistance with the TGA apparatus and the interpretation of the results.

I would also like to express my gratitude to all the people who has given me training and HSE instructions on the different equipment used for this work. This includes TGA training by Eli-Beate Larsen, BET training by Elin Harboe Albertsen, XRD and SEM training by Julian Tolchard, SEM training by Yingda Yu and training on various furnaces by Pei Na Kui.

Abstract

Previous studies have shown that the oxide layer on the surface of silicon particles can reduce the hydrogen evolution that comes from contacting silicon with water during slip casting, prior to nitridation. This study will investigate the effect of the oxide layer on the nitridation of silicon powder.

Silicon powders have been stored at 10°C and 22°C humid atmospheres in two conditions; as received and after a thermal reduction to remove the surface oxide layer. After different storage times, the samples were nitrided using TGA and a large scale furnace. For references some samples were also nitrided in as received condition and after a thermal oxidation.

The nitridation results showed that the samples that were thermally reduced before storage had a lower degree of nitridation than the samples that were stored directly, indicating that the oxide layer had a positive effect on the nitridation. The difference in nitridation between the two storage temperatures were slightly less evident, but results showed that the samples stored at 10°C had a larger degree of nitridation than those stored at 22°C.

XRD analyses showed that most of the silicon nitride product was α-Si_3N_4, usually with an α/β-ratio between 0.8 and 0.9.

A silicon powder of much higher purity was also nitrided for comparison. The results showed that the high purity silicon had a much lower degree of nitridation, indicating that the silicon nitride reaction is very susceptible to impurities in the silicon powder. The α/β-ratio was also lower in the pure silicon.

Sammendrag

Tidligere studier har vist at oksidlaget på overflaten av silisiumpartikler kan redusere dannelsen av hydrogengass som oppstår når silisium kommer i kontakt med vann under slikkerstøping, før nitrering. Dette arbeidet vil undersøke effekten oksidlaget har på nitreringen av silisiumpulver.

Silisiumpulver ble lagret ved 10°C og 22°C grader i fuktig atmosfære. Noe ble lagret direkte i den tilstanden pulveret var da det ble mottatt, mens noe ble termisk redusert for å fjerne oksidlaget, før det ble lagret. Etter å ha vært lagret i forskjellige tidsintervaler ble prøvene nitrert i en TGA og en ovn i større skala. Som referanser ble også noen prøver nitrert i mottatt tilstand og etter en termisk oksidering.

Resultatene fra nitreringsforsøkene viste at prøvene som ble termisk oksidert før lagring hadde en mindre grad av nitrering etter endt forsøk, enn prøvene som ble lagret direkte. Dette er indikasjoner på at oksidsjiktet virker positivt på nitreringen. Forskjellen i nitrering mellom de to lagringstemperaturene var ikke fullt så store, men resultatene viste at prøvene som hadde vært lagret ved 10°C hadde en større grad av nitrering enn prøvene som ble lagret ved 22°C.

XRD analyser viste at mesteparten av silisiumnitriden som ble dannet var α-Si_3N_4 og at α/β-forholdet vanligvis var mellom 0.8 og 0.9.

Et mye renere silisiumpulver ble også nitrert for å ha en sammenlikning. Resultatene viste at det rene silisiumet hadde en mye mindre grad av nitrering, noe som tyder på at silisiumnitridreaksjonen blir svært påvirket av urenheter i silisiumet. α/β-forholdet var også mindre for det rene silisiumet.

Table of Contents

Abbreviations and definitions

- Silica - Silicon dioxide
- CVD - Chemical Vapor Deposition
- BET - Method of measuring the specific surface area of particles
- TGA - Thermogravimetric Analysis
- Large scale furnace - Nitridation furnace used for the nitridation of samples larger than the those possible in the TGA. The term "large" is used in relation to the TGA sizes. Typical sample size for this furnace was ~300 mg.
- SEM - Scanning Electron Microscopy
- FESEM - Field Emission Scanning Electron Microscopy
- EDS - Energy Dispersive Spectroscopy
- XRD - X-ray Diffraction
- Topas - The program used to calculate the amount of each phase present in the XRD scan
- DTA - Differential Thermal Analysis
- DSC - Differential Scanning Calorimetry
- XPS - X-ray Photoelectron Spectroscopy

Chapter 1

Background

1.1 Motivation

Properties such as high thermal shock resistance, good temperature stability and hardness and wear resistance makes silicon nitride very suitable for high temperature applications such as engines, turbines and bearings (Riley, 2000). Another use could be coating of silica crucibles for the solar industry. Advantages using silicon nitride would be easier release of the ingot, minimized stress during solidification and a low contamination of the solar grade silicon.

A commonly used commercial synthesis route for silicon nitride is the direct nitridation of silicon. This is done by heating silicon in a nitrogen containing atmosphere in the temperature range 1150-1450°C.

$$3Si(s) + 2N_2(g) \rightarrow Si_3N_4(s)$$

Although silicon and nitrogen are cheap and abundant elements, the cost of reliable, high purity silicon nitride products are very expensive (Riley, 2000). The silicon nitride reaction is a slow and complex reaction and it is difficult to achieve a microstructure of high quality. A more detailed knowledge of the nitridation process is therefore needed in order to achieve products of higher quality and lower costs.

1.2 Previous work

Many applications of silicon nitride requires a slip casting of the silicon powder before the nitridation. During the slip casting process, the silicon powder comes into contact with water and may react to produce hydrogen.

$$Si(s) + 2H_2O(l) \rightarrow SiO_2(s) + 2H_2(g)$$

The evolved hydrogen can cause porosity in the final product and make it useless for the intended application. Among other factors, the hydrogen evolution will be dependent on the surface oxide layer on the silicon particles. Jørgensen (2011) and Nymark (2012) studied the nature of the hydrogen evolution reaction on the surface of silicon particles when added to water. Nymark (2012) also investigated the effect of storing the silicon powders in humid atmospheres at 10°C and 22°C. She found that a thicker oxide layer gave a lower hydrogen evolution.

1.3 Aim of work

The aim of this work is to continue to study the effect of the humid stored silicon powder. However, this work will not look at the hydrogen evolution reaction, but the effect the storage atmosphere has on the nitridation reaction. Silicon powder samples will be stored for different time periods in 10°C and 22°C humid atmospheres before nitridation. Some samples will also be thermally reduced, to remove the oxide layer entirely, and then stored in the humid atmospheres. As reference points, samples will also be nitrided in as received condition and after a thermal oxidation.

The nitridations will be carried out with a TGA and a large scale furnace. The TGA can precisely log the weight increase that follows the nitridation reaction and will therefore give a good analysis of the reaction. Because the TGA requires very small samples, a larger superkanthal cylindrical furnace will be used to study the nitridation of bigger samples.

The results will be analyzed mainly by XRD and SEM to determine the effects of the humid storage on the nitridation reaction.

Chapter 2

Previous studies on the Si_3N_4-reaction

This chapter will attempt to give a brief overview of important aspects of the silicon nitride reaction. It will also provide the reader with a sufficient foundation to be able to interpret the results presented later and follow in the discussion. The reader might be suspicious to some of the literature cited in this work due to their publish dates. However, there is no reason for concern, the research is still relevant and sited in much newer literature. It might also seem like there is a lot of old literature for this work because the author has chosen to cite the original source as much as possible instead of citing newer articles using the same information over again.

2.1 Elementary properties of silicon

Silicon is a tetravalent atom, which means it is in its most stable state when the valence is 4^+. After oxygen it is the most abundant element in the Earth's crust and makes up 27.7% of the crust by mass. In nature silicon is usually found as an oxide, where it has a more stable valence state. Silicon dioxide, commonly referred to as silica, is one of the most common silicon oxides. When pure silicon is exposed to air at room temperature it will spontaneously oxidize and a thin silica layer will form on the surface (eq. 2.1). It can therefore be assumed that the surface properties of silicon is similar to that of silica (Papirer, 2000).

$$Si(s) + O_2(g) \rightarrow SiO_2(s) \tag{2.1}$$

2.2 Crystal structure of silicon nitride

Glemser et al. (1957) established the existence of two crystalline forms of Si_3N_4; α and β. These two forms were for a long time considered to be the only polymorphs of Si_3N_4, until Zerr et al. (1999) proved the existence of a third polymorph, γ-Si_3N_4. However, this third polymorph requires extremely high temperature and pressure to form and so the focus of this work will be on the more common α and β phases.

According to Hardie and Jack (1957) both α and β have a hexagonal lattice structure where the c-axis of the α-structure is approximately twice that of the β-structure (fig. 2.2.1). The β-structure has been further categorized as having a phenacite structure (Be_2SiO_4), where Be is replaced by Si and O by N. The silicon atoms are placed at the center of tetrahedra with four nitrogen atoms at the corners. The nitrogen are at the center of a trigonal planar geometry linking together three SiN_4 tetrahedra (Ruddlesden and Popper, 1958).

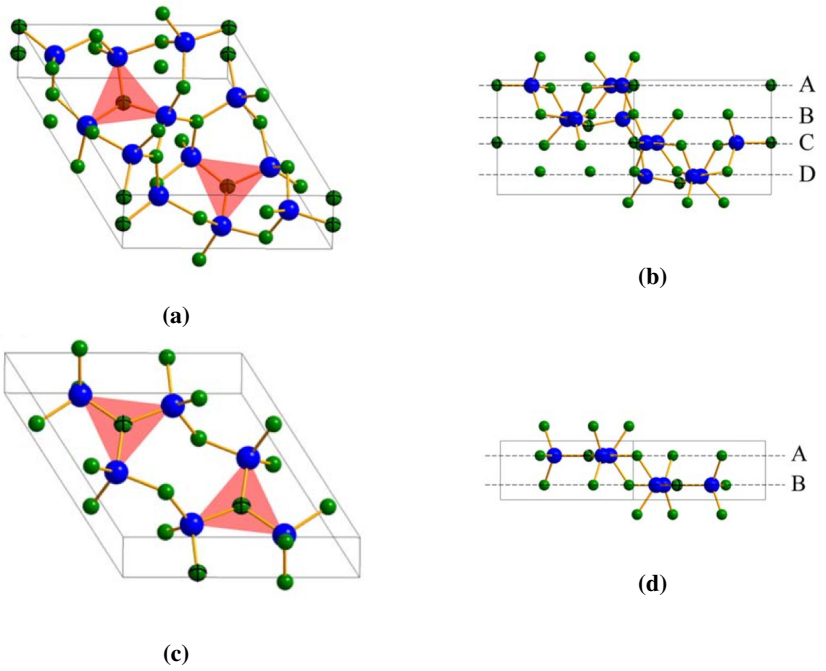

Figure 2.2.1: The different crystal structures of silicon nitride. Blue = Si, green = N. **a**) α-Si_3N_4; **b**) Stacking sequence of α-Si_3N_4 from [1120] direction; **c**) β-Si_3N_4; **d**) Stacking sequence of β-Si_3N_4 from [1120] direction. The trigonal planar geometry linking together the three tetrahedra have been highlighted. The stacking figures show how the α-structure has twice the c-axis of the β-structure (Kuwabara et al., 2008).

Messier (1977) illustrated the structure as gathered rings of alternating silicon and nitrogen atoms. Six of these rings are joined together to form basal planes. Stacking of these basal planes (ABAB...) give the β-structure which comprises Si_6N_8. The β-structure is relatively unstrained and it can be seen that the stacking sequence creates channels with 1.5

Å in radius, which Thompson and Pratt (1967) suggests provides room for large atoms to diffuse (fig. 2.2.2). The α-structure comprises $Si_{12}N_{16}$ and the stacking sequence (ABCD-ABCD...) is similar to that of the β-structure and consists of alternating basal layers of β-Si_3N_4 and a mirror image of β-Si_3N_4, which accounts for the longer c-axis. The α-structure is more distorted than the β-structure and atoms are displaced from idealized positions. The stacking sequence does not create the same channels that can be seen in the β-structure, but the α-structure has voids of relatable size (fig. 2.2.3).

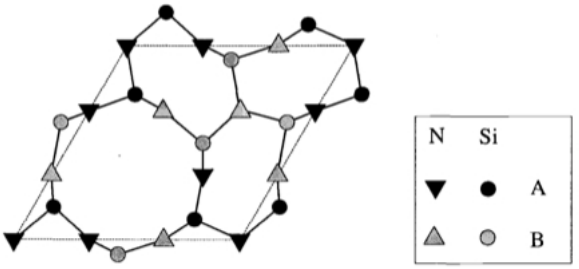

Figure 2.2.2: Basal plane in β-Si_3N_4. Note the open circle which has a radius of 1.5 Å (Pavarajan, 2002)

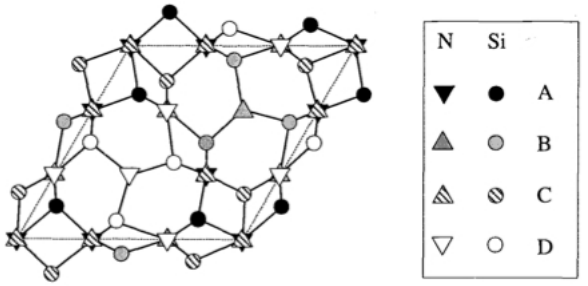

Figure 2.2.3: Basal plane in α-Si_3N_4. Overlapping basal planes does not create the channels seen in the β-structure, but voids of similar size can be seen (Pavarajan, 2002).

2.3 Commercial techniques for synthesizing Si_3N_4

Si_3N_4 is not normally seen in nature, except for trace amounts found in meteorite rocks (Nittler et al., 1995). Silicon nitride can be synthesized in different ways, and the three most commonly used starting materials for industrial purposes are silicon, silica and silicon tetrachloride (Pavarajan, 2002).

The carbothermal reduction and nitridation of silica was the earliest method for Si_3N_4 pro-

duction and is a cost-effective way of creating very pure α-Si_3N_4 powder (Riley, 2000).

$$3SiO_2(s) + 6C(s) + 2N_2(g) \rightarrow Si_3N_4(s) + 6CO(g) \tag{2.2}$$

The reaction is usually carried out between 1200-1450°C depending on the reactivity of the raw material.

The high-temperature decomposition of silicon diimide consists of two steps. First there is the liquid reaction between silicon tetrachloride and ammonia and secondly the decomposition of the silicon diimide which yields amorphous Si_3N_4.

$$SiCl_4(l) + 6NH_3(g) \rightarrow Si(NH)_2(s) + 4NH_4Cl(s) \tag{2.3a}$$

(at 0 °C)

$$3Si(NH)_2(s) \rightarrow Si_3N_4(amorph.) + N_2(g) + 3H_2(g) \tag{2.3b}$$

(at 1000°C)

The amorphous Si_3N_4 can be crystalized to α-Si_3N_4 by heating in nitrogen atmosphere at 1400-1500°C (Riley, 2000).

The direct nitridation of silicon is perhaps the most commonly used synthesis route for Si_3N_4 and will be presented in detail in the next section. The Si_3N_4 created for this paper was done using direct nitridation.

2.4 Direct nitridation of silicon

The direct nitridation of silicon is done by contacting elemental silicon with nitrogen (eq. 2.4) in the temperature range of 1150-1450°C and in ambient pressure.

The overall nitridation reaction is more complex and there has been much debate in the literature regarding the more specific nitridation mechanisms (Moulson, 1979; Jennings, 1983).

The direct nitridation of silicon is a very cheap way to create Si_3N_4 and there is a relatively high tolerance limit when it comes to impurities in the starting silicon. The Si_3N_4 created by this method usually has an α/β-ratio of approximately 90% (Somiya et al., 2003).

2.4.1 Thermodynamic data

The formation of Si_3N_4 from its elements can be described by the following equations:

$$3Si(s) + 2N_2(g) \leftrightharpoons Si_3N_4(s) \tag{2.4}$$
$$\Delta G_{2.4} = -723 + 0.315 \text{TkJmol}^{-1}$$

$$3Si(l) + 2N_2(g) \leftrightharpoons Si_3N_4(s) \tag{2.5}$$
$$\Delta G_{2.5} = -874 + 0.405 \text{TkJmol}^{-1}$$

$$3Si(g) + 2N_2(g) \leftrightharpoons Si_3N_4(s) \tag{2.6}$$
$$\Delta G_{2.6} = -2080 + 0.757 \text{TkJmol}^{-1}$$

The large and negative value of the first term in these equations indicate that they are very exothermic. The free energy of formation was calculated by Moulson (1979) and based on data gathered by Pehlke and Elliot (1959). The research by Pehlke and Elliot (1959) included both α and β phases and so equations 2.4-2.6 does not refer to any specific crystalline form.

Myhre (1989) suggests that the α-structure has a slightly higher free energy than the β-structure, due to its more distorted structure. This is supported by the observation that α-Si_3N_4 recrystallizes to β-Si_3N_4 during sintering. Riley (2000) refers to the difference in Gibbs free energy between α and β as being approximately 30 kJmol^{-1} at room temperature.

2.4.2 The Si-O-N system

The Si-O-N system was thoroughly studied by Blegen (1975, 1976) and is still cited in much litterature. The stability phases for the system was described by the following equations:

$$Si(s) + O_2(g) \leftrightharpoons SiO_2(s) \tag{2.7}$$

$$2Si(s) + \frac{1}{2}O_2(g) + N_2(g) \leftrightharpoons Si_2ON_2(s) \tag{2.8}$$

$$Si_2ON_2(s) + \frac{3}{2}O_2(g) \leftrightharpoons 2SiO_2(s) + N_2(g) \tag{2.9}$$

$$2Si_3N_4(s) + \frac{3}{2}O_2(g) \leftrightharpoons 3Si_2ON_2(s) + N_2(g) \tag{2.10}$$

$$3Si(s) + 2N_2(g) \leftrightharpoons Si_3N_4(s) \tag{2.11}$$

Using Gibbs free energy from the reactions, Giridhar and Rose (1988) calculated the stability regions of the phases at 1250°C as a function of the oxygen and nitrogen partial pressures (fig. 2.4.1a). It can be seen from the figure that if we have a nitrogen pressure of 1 atm, we need to have a p_{O_2} lower than 10^{-22} atm in order to form stable Si_3N_4. This is an extremely low oxygen partial pressure. Typical commercial gas-mixtures comes with O_2 and H_2O contaminants in the ppm range, which would give a p_{O_2} of 10^{-6} atm Giridhar and Rose (1988) therefore proposed to include the process of active oxidation in the calculation of the stability phases in the Si-O-N system. In addition to reactions 2.7-2.11 they also included the following reactions:

$$SiO_2(s) + Si(s) \leftrightharpoons 2SiO(g) \tag{2.12}$$

$$Si_2ON_2(s) \leftrightharpoons Si(s) + SiO(g) + N_2(g) \tag{2.13}$$

$$Si_2ON_2(s) + SiO_2(s) \leftrightharpoons 3SiO(g) + N_2(g) \tag{2.14}$$

$$3Si_2ON_2(s) \leftrightharpoons Si_3N_4(s) + 3SiO(g) + N_2(g) \tag{2.15}$$

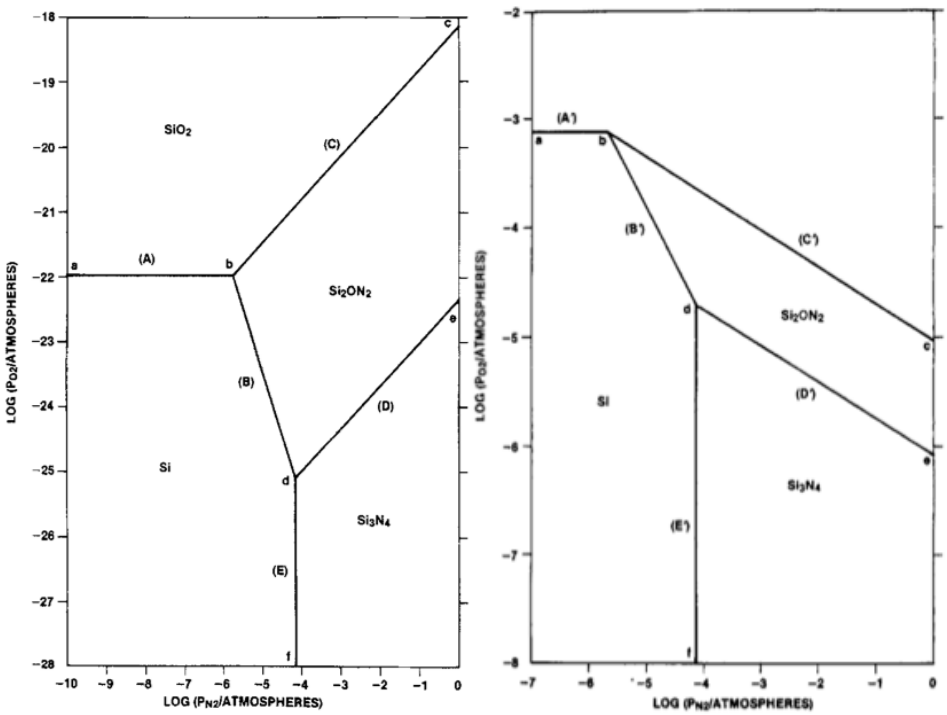

(a) **(b)**

Figure 2.4.1: Stability field diagrams for the Si-O-N system. **a**) Calculations are based on reactions 2.7-2.11; **b**) Calculations include the process of active oxidation and are based on reactions 2.7-2.15. When including the process of active oxidation in the calculations Si_3N_4 becomes stable for p_{O_2} as high as 10^{-5} atm (Giridhar and Rose, 1988).

Figure 2.4.1b shows that pure Si_3N_4 will be stable at oxygen pressures as high as 10^{-5} atm, which seems to be a more realistic partial pressure. Giridhar and Rose (1988) therefore concludes that active oxidation is a criterion for the formation of Si_3N_4.

2.5 Factors influencing the direct nitridation of silicon

There are several factors which influence the nitridation of silicon, such as particle size, reaction temperature, heating rate, reaction time, reaction gas composition, metal impurities in the silicon and the silicon surface oxide layer. The effect of these variables on nitridation rate, α/β-ratio and microstructure have been extensively studied over the years (Campos-Loriz and Riley, 1978; Boyer and Moulson, 1978; Sangster, 2005) . Due to the complexity of the reaction and the interdependence between reaction variables, the Si/N_2 reaction still holds many unanswered questions.

2.5.1 Self-diffusion in Si_3N_4

It was early documented (Parr et al., 1960) that the formation of extremely thin, intact, layers of Si_3N_4 would choke off any further reaction. The high strength of the Si_3N_4 chemical bonds and the difficulty in sintering powder samples indicate that lattice diffusion in Si_3N_4 is very slow (Riley, 2000). Sangster (2005) states that the current opinion of the field is that the available self-diffusion data excludes Si/N_2 reaction mechanisms which involves solid state diffusion through Si_3N_4.

The nitrogen self-diffusion were measured with a gas-solid isotope exchange technique, using ^{15}N as a tracer. The measurements were performed by Kijima and Shirasaki (1976) and were done on polycrystalline α -and β-Si_3N_4 between 1200°C and 1410°C. When correcting for grain boundary diffusion they obtained the following diffusion coefficients:

$$D_{N_\alpha} = 3.7 \times 10^{-8} exp(-233 kJmol^{-1}/RT) \quad [m^2 s^{-1}] \tag{2.16}$$

$$D_{N_\beta} = 6.8 \times 10^{10} exp(-777 kJmol^{-1}/RT) \quad [m^2 s^{-1}] \tag{2.17}$$

As Riley (2000) points out, there is a large difference in the two activation energies and the α energy is very low, suggesting that there might be some errors in the measurements. It is recognized that the difficulty in obtaining pure α and β crystals, together with the volatility of Si_3N_4 during high temperature diffusion anneals, makes these measurements very difficult. However, a more recent study of silicon diffusion in α-Si_3N_4 found the silicon diffusion coefficient to be approximately

$$D_{Si_\alpha} = 1 \times 10^{-19} exp(-197 kJmol^{-1}/RT) \quad [m^2 s^{-1}] \tag{2.18}$$

The measurement was done within the temperature range 1400-1600°C and also shows a low activation energy. Riley (2000) therefore concludes that although there are significant

differences in the measured data, the values are consistent with the recognized lack of mobility of silicon and nitrogen in the Si_3N_4 lattice. He also suggests that nitrogen diffusion might be rate controlling in the Si_3N_4 gas/solid reaction. The diffusion coefficients are plotted in figure 2.5.1.

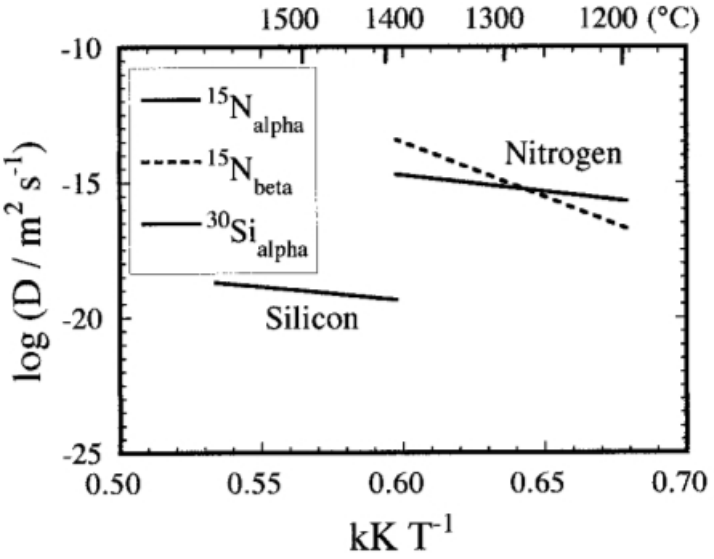

Figure 2.5.1: Silicon and nitrogen diffusion coefficients in Si_3N_4 (Riley, 2000).

At higher temperatures D_N is higher for β -than for α-Si_3N_4, which may indicate differences in vacancy formation energies according to Kijima and Shirasaki (1976). Jennings (1983) argues that the hexagonal channels in the β-structure (section 2.2) should allow the diffusion of atomic nitrogen and could therefore account for a higher diffusion rate. However, there is no evidence of this phenomenon and the prevailing opinion seems to be that there is no reason to expect anything but extremely low diffusion through the channels (Sangster, 2005).

2.5.2 Effects of impurities

The effects of impurities on the nitridation reaction has been extensively studied in much literature, especially the effect from iron impurities (Popper and Ruddlesden, 1961; Atkinson et al., 1976; Boyer and Moulson, 1978). Iron is suspected to help disrupt the silica surface layer and allow the escape of SiO(g) from the reaction at the Si/SiO_2 interface. The formation of local, low temperature, melting points with an $FeSi_x$ composition is expected to aid the formation of β-Si_3N_4 (Boyer and Moulson, 1978). The effect of impurities is beyond the scope of this work, but generally it can be said that the silicon nitride reaction is extremely sensitive to impurities in the silicon powder (Riley, 2000).

2.5.3 Effects of the SiO_2 surface layer

There is general agreement in the literature that the SiO_2 surface layer hinders the access of nitrogen to the silicon surface and the volatilization of silicon, and therefore have a retarding effect on the nitridation (Dervisbegovich and Riley, 1981; Rahaman and Moulson, 1984). It is still possible for nitridation to occur to some extent by diffusion through the oxide layer as was shown by Kooi et al. (1976). The silicon nitride layer then formed act as a barrier against silicon diffusion, preventing further nitridation.

In order to achieve an appreciable amount of nitridation, the first step in the nitridation process must be removal of the SiO_2 layer on the particles. Some methods to achieve this are:

i) Vacuum pre-treatment at 1000-1200°C. The following reaction was proposed by Atkinson et al. (1976):

$$SiO_2(s) \rightarrow SiO(g) + \frac{1}{2}O_2(g) \tag{2.19}$$

ii) During vacuum pre-treatment of silicon powder at 1200-1300°C Blegen (1976) proposed the following reaction:

$$SiO_2(s) + Si \rightarrow 2SiO(g) \tag{2.20}$$

iii) Campos-Loriz and Riley (1979) suggested the following equation for removal of SiO_2 by use of hydrogen:

$$SiO_2(s) + H_2(g) \rightarrow SiO(g) + H_2O(g) \tag{2.21}$$

Older literature (Atkinson et al., 1976; Pigeon and Varma, 1992) reports the SiO_2 surface layer to be approximately 3 nm. In a more recent work, Nymark (2011) estimated the oxide thickness by XPS analysis and found it to be 0.7 nm. The powder used in this work is the same quality as that studied by Nymark (2012), although from a different sample batch.

Atkinson et al. (1976) observed that silicon powder with deliberately thickened SiO_2 layers highly retarded the nitridation reaction, and when the thickness reached ~1 μm, the reaction was completely halted. Furthermore they concluded that an increased reaction temperature and reduced nitrogen pressure encouraged the growth of thick SiO_2 layers. This is in agreement with Giridhar and Rose (1988) who proposed that thermal nitridation of silicon will only occur under conditions promoting active oxidation, that is, formation of SiO(g) rather than SiO_2(s, l) (section 2.4.2). The role of SiO(g) in the nitridation of silicon is one of the reaction mechanisms which is still not fully understood and it will be discussed in more detail in the next section.

2.5.4 Si(g) and SiO(g) reactions

The conversion of silicon to Si_3N_4 follows a theoretical weight gain of 66.49%. However, as Billy (1959) was the first to indicate, this theoretical weight gain is not observed. Usually the total weight gain is about 5% less than the theoretical, especially in experiments with flowing gas (Popper and Ruddlesden, 1961). This observation indicate the volatility of the Si-O-N system.

There are two possible gas phase reactions (CVD processes) for forming Si_3N_4 (Campos-Loriz and Riley, 1976; Dervisbegovich and Riley, 1981):

i) $3Si(g) + 2N_2(g) \rightarrow Si_3N_4(s)$

ii) $3SiO(g) + 2N_2(g) \rightarrow Si_3N_4(s) + \frac{3}{2}O_2(g)$

In his review Sangster (2005) states that there is still debate in the literature, regarding which of these reactions are the primary nitridation process.

Arguments for Si(g) are first of all that reaction (ii) is not thermodynamically feasible (ΔG = 502 $kJmol^{-1}$; Moulson, 1979) and that it is kinetically unfavored because the removal of O_2 from Si_3N_4 formation sites is many orders to low (Dawson and Moulson, 1978). Secondly, the evaporation rate of Si(g) is 10^{-6} $kgm^{-2}s^{-1}$ at 1350°C, which is sufficient to sustain the reaction rate of $\sim 10^{-7}$ $kgm^{-2}s^{-1}$ (Moulson, 1979; Pigeon and Varma, 1992). In comparison with unlimited access to Si(g) it seems unlikely that SiO(g) is a significant nitridable species. Sangster (2005) concludes that literature until 1986 holds unanimity on the point that α-Si_3N_4 is formed via reaction (i).

In a later review Riley (1989) states that Si(g) and SiO(g) are both contributing effectively to the nitridation and that they are interchangeable dependent on the conditions. SiO(g) generated from the Si(s)/SiO_2(s) interface leads to α-Si_3N_4 and when adding H_2 to the nitriding gas, the morphology changes from the thicker CVD to the thinner whisker form (Moulson, 1979). If H_2 is added, reaction (ii) might go by formation of H_2O (Dawson and Moulson, 1978). Although the SiO(g)/N_2 reaction is not significant under normal nitriding conditions, it might become so during the early stages of the nitridation due to volatilization of SiO_2 (Moulson, 1979).

2.6 Formation of α- and β-Si_3N_4

Upon formation Si_3N_4 follows a ~22% volume expansion, yet the external dimensions remains practically the same (Jennings, 1983). This means that as the reaction proceeds inward, no solid material is pushed outwards. The reaction must therefore occur in the voids between particles or in developing pores inside the particles (figure 2.6.1). This also means that silicon has to be transported away either as vapor or liquid. When a pore has been developed the reaction can proceed on the newly created surface. When a thin product layer is formed, the reaction can only proceed if silicon is transported to the reaction cite. Jennings (1983) concludes that the silicon species must be either vapor or liquid on account of the low diffusion rates in Si_3N_4 (figure 2.5.1).

The bonding between silicon and nitrogen is 70% covalent in nature, which is likely what gives Si_3N_4 its high mechanical strength and makes it hard to sinter (Riley, 2000).

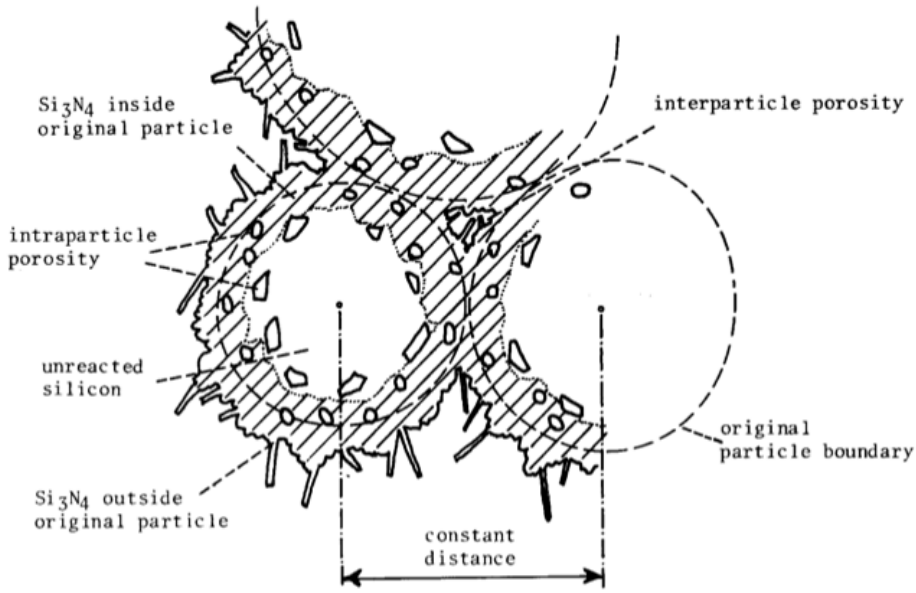

Figure 2.6.1: The figure depicts the reaction of silicon particles with nitrogen. Product growth is dependent on inter- and intraparticle porosity as it advances towards the center of particles. As Si_3N_4 growth continouos, the outer dimensions remain unchanged (Jennings, 1983).

2.6.1 Simultaneously formation of α- and β-Si_3N_4

There is general agreement in the literature that the reaction between Si(s) and N_2(g) produces a mixture of α- and β-Si_3N_4. Dalgleish et al. (1980) investigated the reaction of mono-crystalline Si(100) and Si(111) with N_2 at 1350°C and observed a general mixture of α and β. They concluded that there is a kinetic competition with conditions, allowing the formation of both phases. Investigations by Jennings and Richman (1975) showed that nitridation of high purity silicon powder in nitrogen at 1350-1450°C produced a mixture of α and β. It has also been shown (Gregory and Richman, 1982) that reaction in the lower temperature range (1100-1360°C) yields a mixture of α and β.

According to Sangster (2005), if either α -or β-Si_3N_4 is favored under initial nitriding conditions, seeds of that phase will form. The formation of these seeds will strongly affect the outcome of the reaction regardless whether another α/β ratio is preferred in the later stages of the reaction process. Nitridations of Si(99.3%) in high purity nitrogen at 1347°C and 1367°C done by Albano et al. (1991) showed that both α and β forms during the low reaction temperatures and that β is the dominant form during higher reaction temperatures (figure 2.6.2). Morgan (1980) observed that slow heating through the lower reaction temperature range, gave mostly α-Si_3N_4 even though most of the reaction occurs

at higher temperature. This seems to explain why most silicon nitride have a higher α than β fraction.

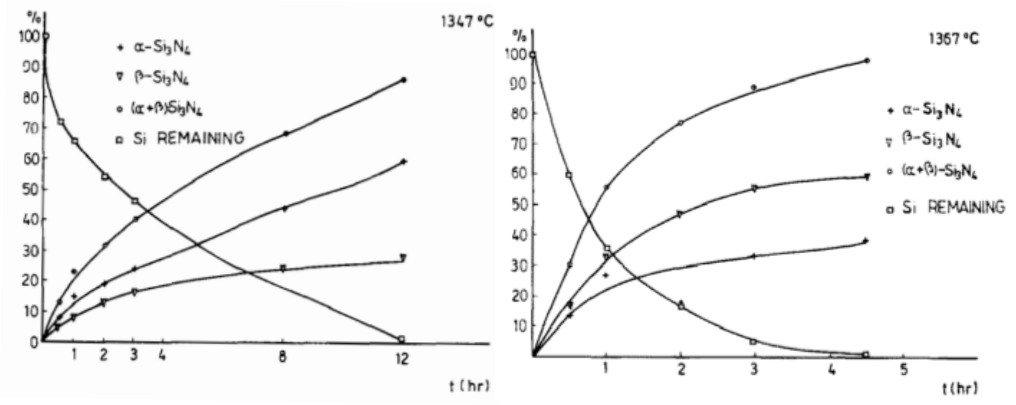

(a) **(b)**

Figure 2.6.2: Nitridation with Si (99.3%) and high purity N_2 at **a**) 1347°C and; **b**) 1367°C. The samples were heated at 10°C/min to the reaction temperatures. A high reaction temperature favors β-Si_3N_4, rather than α-Si_3N_4 (Albano et al., 1991).

2.6.2 Formation of α-Si_3N_4

As observed by Morgan (1980), α-Si_3N_4 preferentially forms at 1000-1250°C. Hojo et al. (1975) also found that α-Si_3N_4 forms preferentially at lower nitrogen partial pressures (figure 2.6.3).

The growth of α-Si_3N_4 is usually a characteristic whiskery matt (Dalgleish and Pratt, 1973; Moulson, 1979), although hexagonal prisms and platelets also occur (Morgan, 1980). The formation of the whiskers is a strong indicator of a vapor-phase reaction and so the formation is dependent on the surface area of the silicon powder, because the formation occurs on solid surfaces (Campos-Loriz and Riley, 1978). As stated in section 2.5.4 the formation of α-Si_3N_4 is often attributed to reaction (ii), although there are still some uncertainty regarding the amount formed from this reaction. It is a testimony to the complexity of the Si/N_2 reaction that most literature agrees on α-Si_3N_4 being a product of gas reactions, where reactants have the highest degree of freedom, yet the α-structure is more strained than the β-structure (Jennings, 1983). Jennings (1983) believes the formation of α-Si_3N_4 comes from molecular nitrogen, while the β formation is via dissociated atomic nitrogen. This theory is supported by Pigeon et al. (1993).

Jones and Lindley (1976) reported that the amount of α-Si_3N_4 could be reduced by increasing the reaction gas flow rate which would carry away SiO(g) from reaction sites.

Riley (1989) stated that, in general, all nitridations below 1400°C would form mainly α-Si_3N_4.

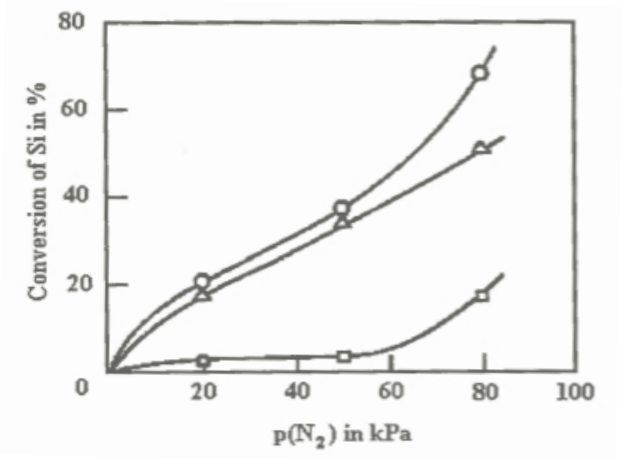

○ = fraction reacted
△ = conversion to α-Si_3N_4
□ = conversion to β-Si_3N_4

Figure 2.6.3: p_{N_2} dependence for conversion of Si (99.5% or 99.99% purity) to α- and β-Si_3N_4 during 8 hours at 1380°C. β-Si_3N_4 is clearly favored at higher nitrogen partial pressures (Hojo et al., 1975).

2.6.3 Formation of β-Si_3N_4

Morgan (1980) observed that β-Si_3N_4 dominates at 1390°C and that it increases with increasing p_{N_2} at 1380°C (figure 2.6.3). Longer nitridation time will also lower the α/β ratio (Guthrie and Riley, 1973).

In section 2.4.1 it was mentioned that α-Si_3N_4 can re-crystalize to β-Si_3N_4, albeit this is true, it requires long heat treatment above 1500°C (Messier et al., 1978). Hojo et al. (1975) showed that β-Si_3N_4 is mainly formed by the direct reaction Si/N_2 and not by recrystallization.

When the SiO_2 surface layer is gone, β-Si_3N_4 formation will account for most of the Si_3N_4 (Campos-Loriz and Riley, 1976). Jennings and Richman (1975) observed that under conditions favoring β-Si_3N_4, a Si_3N_4 shell would form on the surface of the silicon particles. When the surface has been covered, spikes will then start to grow into intraparticle voids as shown in figure 2.6.4. The reaction rate will follow a linear law as long as there is room for the spike to grow. In the end the spikes will grow into what appears to be a single grain with a high dislocation density (Jennings, 1983).

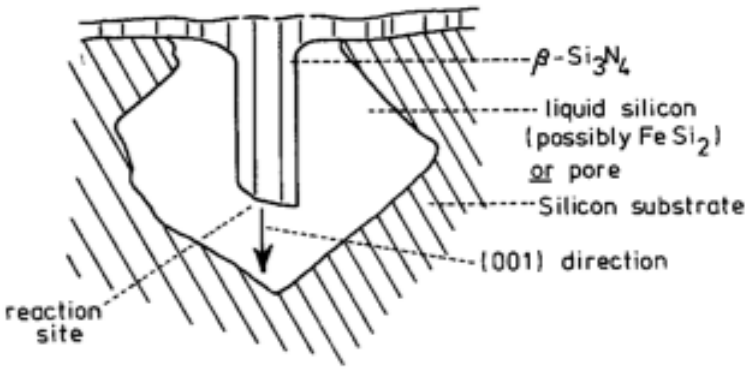

Figure 2.6.4: Facetted β-Si_3N_4 growth into liquid silicon or a pore. The growth continues until there is no more room for it to grow. Nitrogen is supplied either through liquid silicon or diffusion through the spike. In the latter case the spike will be relatively short due to slow diffusion rates (Jennings, 1983).

Even though there have been reports of β-Si_3N_4 forming via gas phase reactions, the growth of hexagonal prisms from liquid silicon is well established (Morgan, 1980). Sangster (2005) reports of a widely agreement on the major growth formation of β-Si_3N_4 from liquid phases. Impurities may enhance the formation of β-Si_3N_4 either by creating local melting sites or by removal of the SiO_2 surface layer (Moulson, 1979).

2.6.4 Nitridation mechanisms

Sangster (2005) classifies the proposed nitridation mechanisms into four groups. 1) nucleation and lateral growth of dense Si_3N_4 layers with silicon particles ≥ 100μm; 2) nitrogen diffusion through porous Si_3N_4 product layers, silicon particles are 5-37 μm; 3) growth by surface exposure due to nitride layer cracking and exfoliation on ~2 μm particles; 4) nucleation and preferential growth mechanism for ~ 0.2 μm particles. The two former mechanisms are more relevant to this study, due to their bigger particle size, and will be discussed in more detail in the following sections.

Nucleation and lateral growth

Many workers (Atkinson et al., 1976; Moulson, 1979; Jennings, 1983) have reported that in the absence of a substantial oxide layer on the silicon surface, the initial reaction is a nucleation and growth process. Moulson (1979) made a reaction model to describe the reaction between pure silicon and nitrogen (figure 2.6.5). The first stage of the reaction is the formation of Si_3N_4 nuclei on the surface of silicon. Certain points on the silicon surface seems to be favored and nitride nucleation occurs predominantly on these sites (Riley, 1983). The growth rate and size of the crystals are strongly related to the temperature

and nitrogen partial pressure. The nuclei proceeds to grow both laterally and vertically as silicon is supplied by a combination of surface diffusion and evaporation. Pores and cavities form due to the evaporation of silicon and provides new surface for Si_3N_4 to form. As the growth continues the free silicon surface area decreases and diffusion distances increases which slows the reaction down. Eventually a Si_3N_4 film covers the entire surface area and the reaction rate falls to nearly zero.

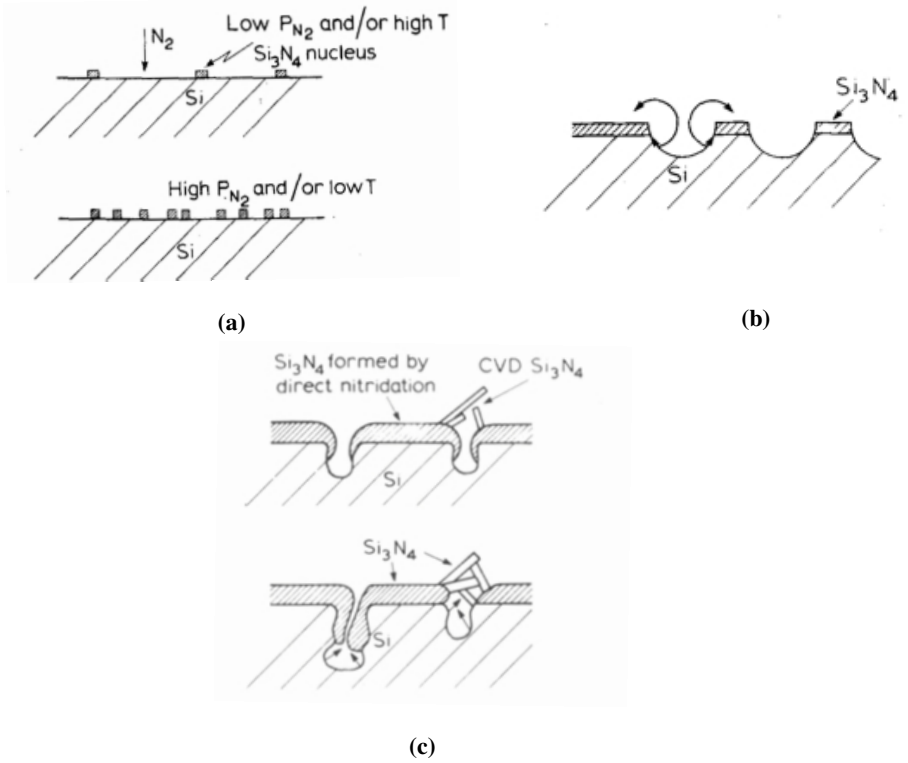

Figure 2.6.5: Different stages in the reaction between pure Si and N_2; **a)** Formation of Si_3N_4 nuclei on the Si surface. The nucleation density increases at higher p_{N_2} and/or lower temperature; **b)** The growth of the nuclei is both laterally and vertically. The supply of silicon to growth sites are a combination of surface diffusion and evaporation. For $p_{N_2} < 1$ atm, the rate of N_2 arrival to growth sites determines the rate of reaction; **c)** As free surface area decreases, direct nitridation slows as a result of further diffusion lengths. CVD reactions of Si(g) continues. Eventually effective separation of reactants give a reaction rate close to zero (Moulson, 1979).

According to Sangster (2005) the different stages of nitridation of high purity silicon powder can be described fairly well by three different rate laws. The "induction" period noticed in some cases can be related to the time it takes for the surface oxide layer to evaporate (Riley, 1983). The second stage (figure 2.6.4a-2.6.4b) displays a linear nitridation rate which, in the absence of impurities and surface SiO_2, is proportional to the nitrogen partial pressure, (Moulson, 1979). The reaction rate in the third stage (figure 2.6.4c) moves from a linear to an asymptotic rate as the reaction falls to nearly zero.

N_2 diffusion through Si_3N_4 product

In their nitridation experiments on silicon particles from 5-37μm, Pigeon and Varma (1992) stated that in order to achieve a full nitridation, the Si_3N_4 product layer had to "maintain reasonable microscopic porosity, albeit small ($\ll$ 1μm), throughout the course of the reaction)." This can be found as micropores in the α-matte and whiskers and as open channels in the c-direction of the β-structure, the latter are expected to contribute at a much slower rate. As long as these pores exist the reaction will continue inwards to the center of the silicon particle until the Si_3N_4 product is thick enough to restrict further nitrogen diffusion (Pigeon and Varma, 1992; Pigeon et al., 1993).

Chapter 3

Experimental

3.1 Overview of the silicon powder

Table 3.1.1 shows an overview of the two different silicon powder samples used for this work. The powder was supplied by Elkem AS. The focus of this work has been on the powder designated "Batch A" which contains a considerable amounts of impurities compared to "Batch B".

Table 3.1.1: Overview and chemical analysis of the silicon powder supplied by Elkem AS.

Sample (Ref. name)	*Size [µm]*	*Mech. treat.*	*Si [wt%]*	*Fe [wt%]*	*Al [wt%]*	*Ca [wt%]*	*Ti [wt%]*
Batch A	0-75	Milled	99.5	0.135	0.215	0.025	0.013
Batch B	0-75	Milled	99.9	<0.0001	<0.0001	<0.0001	<0.0001

3.1.1 Surface area measurements

The surface area of the silicon particles were measured in a Tristar 3000 from Micromeritics, which uses the adsorption of nitrogen onto the particles in order to find the surface area. Before the measurements could start, the powder was set to degas at 250°C overnight to remove humidity and volatile species. The sample was weighed before and after the degassing to check for possible weight loss.

The sample holder was fitted with an isothermal jacket and placed in a cold bath inside the Tristar 3000 machine. Liquid nitrogen was used to keep a low temperature in the cold bath throughout the measurement.

In order for the measurements to be as precise as possible, the sample holder was only touched with cotton gloves or lint free cloth during the entire procedure.

The 5-point BET method was used to measure the adsorption of nitrogen onto the particles. The average surface area of the particles were then calculated using the BET-method, under the assumption of spherical particles (Brunauer et al., 1938).

3.2 Experimental procedure

Figure 3.2.1 shows the different experimental procedures leading up to nitridation. The different preparation methods will be explained in the next section, while this section will focus on explaining the logic behind the sample codes given to the different samples. This is necessary because the tables presented in the results could not fit all the necessary information about the samples without the codes. Samples have therefore been given a sample code based on their route to nitridation. If a sample was nitrided directly from batch A, i. e. "As Received," it would have the sample code A-AR-S.1. So "A-AR" means that it is from batch A and that it is nitrided in as received condition. "S" is for "small" and means the sample was nitrided with a TGA apparatus whereas an "L" would stand for "large" and mean that the sample was nitrided in a large scale furnace. Sometimes several parallels were carried out and so the number behind the "S" or "L" refers to the sample's number in the parallel.

If the sample was thermally oxidized before nitridation it would be named A-TO-S.1 (Batch A-Thermally oxidized-"Small scale" TGA nitridation parallel no.1).

If the sample was kept in humid storage for a number of days before nitridation it would be named A-22D.4-S.1. 22D.4 means the sample was stored at 22°C in a humid atmosphere for 4 days before nitridation. Similar if it was stored at 10°C it would be called A-10D.4-S.1.

The last nitridation path consisted of a thermal reduction of the silicon in a H_2/Ar atmosphere before either direct nitridation or humid storage. A sample which was stored for 2 days at 10°C after thermal reduction and prior to nitridation would be called A-H2-10D.2-S.1 and A-H2-D.0-S.1 if it was nitrided without any days in humid storage.

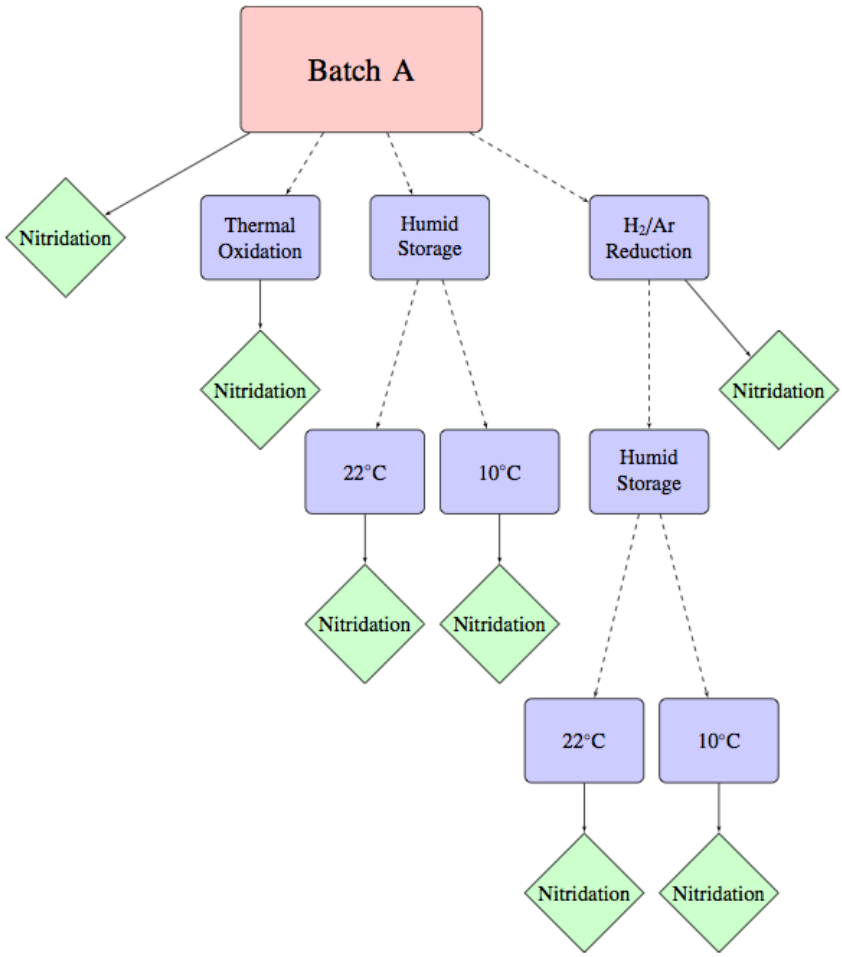

Figure 3.2.1: Flowchart showing the different preparations done to samples prior to nitridation. The preparations before nitridation is the logic behind the sample codes. A sample that have been thermally reduced in H_2/Ar and then stored at 22°C for 30 days before nitridation would be called A-H2-22D.30-S.1. S-1 means it was nitrided in the TGA and it was sample number 1. Ideally, samples would be stored for 1,2,4 and 30 days before nitridation.

3.3 Preparation of the silicon powder

3.3.1 Thermal oxidation

The thermal oxidation of the silicon powder was done in a LabStar calcining furnace. The powder was placed in an open Al_2O_3 sample ship and spread to approximately 1-2 mm thickness to ensure oxidation of the entire sample. The sample was heated at 200°C/h to the desired temperature of 900°C where it was kept for 1 hour.

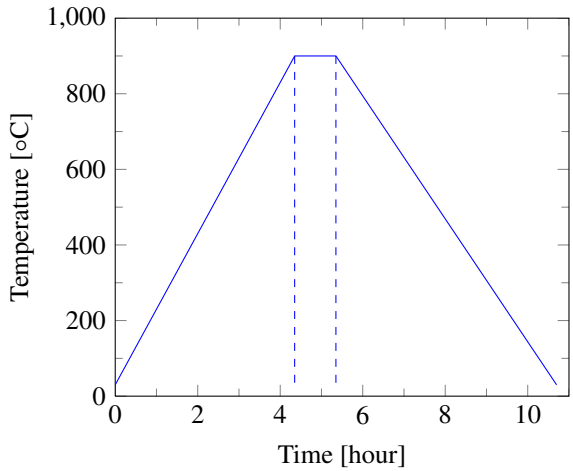

Figure 3.3.1: Temperature program for the oxidation of silicon powder. The sample was heated in air at 200°C/h to 900°C where it was kept for 1 hour before being cooled at 200°C/h.

3.3.2 Humid storage

The storage and exposure of silicon powder to humid atmospheres is the same set-up as that used by Nymark (2012) when she studied the effect the storage conditions had on hydrogen evolution at the silicon surface when in contact with water. The silicon powder samples were put in open petri dishes and placed into sealed containers. The containers contained a beacon of water which gave a humid atmosphere. For the 22°C storage, the containers were placed inside an incubator. 10°C were obtained by placing the containers in a wine cooler. Both the storage rooms had a measurement error of ±1°C.

The saturation vapor pressures were calculated by Nymark (2012) and found to be 0.026 atm in the incubator and 0.012 atm in the wine cooler. Care was taken to ensure that the petri dishes were placed away from the container walls in case the water should condense.

3.3.3 Thermal reduction and removal of the oxide surface layer

For the removal of the SiO_2 surface layer, a super kanthal furnace was used (figure 3.4.3). Two different heating programs were used for this procedure. For the first program the sample was heated to 1200°C at 200°C/h where it was kept for 10 hours before cooling down to room temperature at the same rate. Some uncertainty existed as to whether the oxide layer had been completely removed and so the next sample batch was heated to 1300°C instead of 1200°C.

For both the programs the silicon was placed in an open Al_2O_3 sample ship and heated at 200°C/h to the desired temperature, as shown in figure 3.3.2.

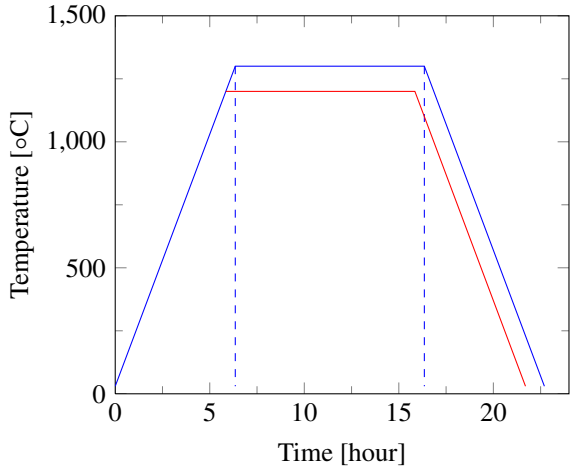

Figure 3.3.2: Temperature program for removal of the SiO_2 surface layer. The blue line represent the most used program which were heated to 1300°C at 200°C/h and kept at this temperature for 10 hours. The other temperature program (red line) was used on some samples and is exactly the same except the reaction temperature is 1200°C instead of 1300°C.

3.4 Nitridation of the silicon powder

The nitridation of the silicon powder was carried out in two different furnaces, one for a small and accurate measurement of the nitridation process and one for a nitridation of larger samples. The equipment have different limits when it comes to the heating rates, so it was necessary to use two different heating programs. In both cases, 1330°C was the reaction temperature and the samples were kept here for 2 hours. The nitridation gas was 50%N_2 and 50%Ar.

3.4.1 TGA

TGA is a method which accurately measures differences in sample weight as a function of time and temperature. For the TGA samples prepared in this work a Netzsch STA 449C Jupiter was used. The apparatus allows the use of other atmospheres in addition to air.

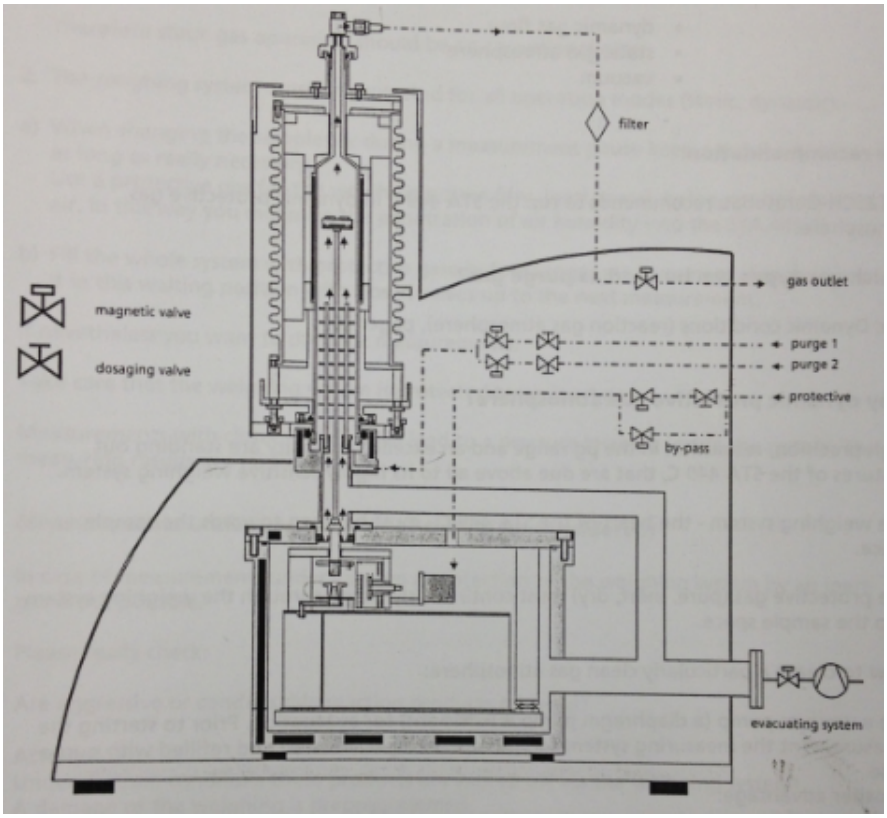

Figure 3.4.1: The figure shows the gas flow diagram for the TGA apparatus. The gas flow is admitted from the bottom of the sample chamber and flows up, around the sample crucible and a reference crucible, before it is admitted from the top of the chamber (Netzsch, STA 449C Jupiter instruction manual).

Approximately 20 mg samples were placed in an Al_2O_3 crucible, filling it about one third. Before the measurement could start, oxygen had to be evacuated from the sample chamber, which was then filled back up with argon. This was done three times to make sure any residual oxygen was removed. Nitrogen and argon were then allowed into the sample chamber to be mixed, at 20 mL/min each.

It should be noted that at some point during the experimental work, the Pt-element on which the crucibles are placed, broke and had be replaced. For the rest of the measure-

ments a DTA set-up was used. This set-up requires a different crucible, which is a bit deeper and so the samples used from this point was approximately 35 mg. To ensure that the Pt-element would not be damaged again, the gas flow was increased to a total of 60mL/min. For future reference it should be mentioned that the old set-up was DSC.

A background measurement must be done in order to obtain a precise analysis . For this measurement, the program is run with an empty sample holder. The background measures the effect of the expanding gas, which can then later be withdrawn from the actual measurement.

The heating program is shown in figure 3.4.2. The nitridation reaction is expected to start at 1150°C which is why the heating rate is slowed down to 2°C/min at 1100°C.

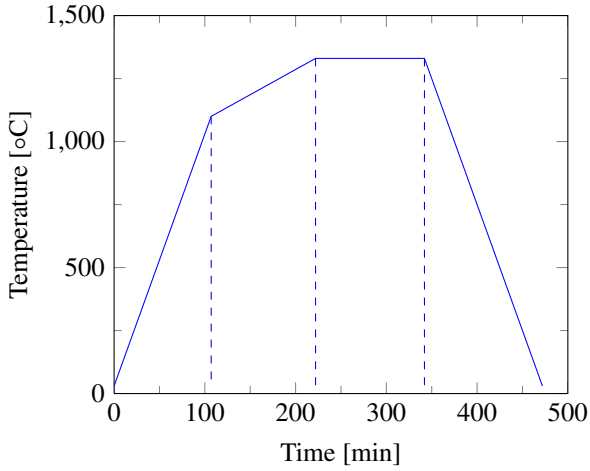

Figure 3.4.2: Temperature program for nitridation in the TGA equipment. The samples were heated to 1100°C at 10°C/min. The heating continued at 2°C/min to the reaction temperature of 1330°C, where the samples were kept for 2 hours before cooling at 10°C/min.

3.4.2 Large scale nitridation

The TGA is limited to very small sample batches, so in order to investigate samples of a larger scale, a super kanthal cylindrical furnace was used. It should be noted that the word "large" is used in relation to the TGA scale which is very small. Typically, samples nitrided in this furnace were around 300 mg.

There is no electronic logging of these experiments so the samples had to be measured carefully before and after each experiment. The samples were placed in an Al_2O_3 sample ship and placed inside the cylindrical Al_2O_3 tube furnace. The gas was admitted from one side of the tube and escaped from the other side (figure 3.4.3). It was not possible to remove oxygen by evacuation before admitting the reaction mixture of N_2/Ar. The

sample chamber was therefore flushed with the reaction gas for some time, before the measurements were started. The gas was admitted at approximately 15mL/min.

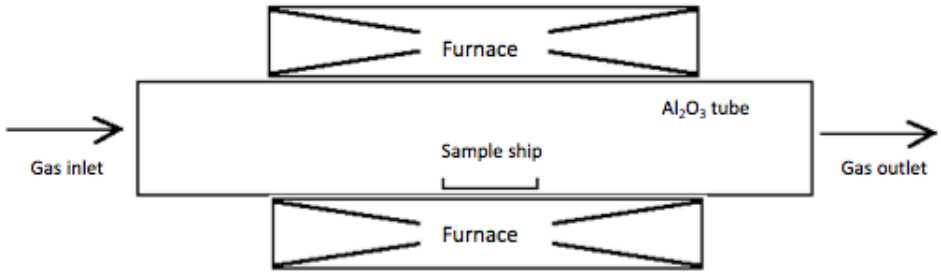

Figure 3.4.3: The figure shows a schematic of the gas flow and the position of the sample ship in the large scale nitridation furnace. The picture was constructed for this work.

Figure 3.4.4 shows the temperature program that was used for this furnace. As can be seen, the heating rate is slightly different from the one used in the TGA. The heating rate is 200°C/h up to 1100°C, then the heating rate is slowed to 120°C/h. At 1330°C there is an isothermal step of two hours, before the sample is cooled to room temperature at 200°C/h.

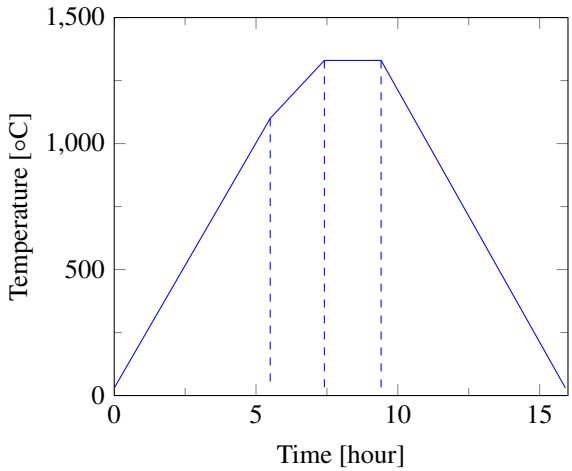

Figure 3.4.4: Temperature program for the large scale nitridation. The initial heating rate is 200°C/h to 1100°C, followed by a slow heating of 120°C/h to 1330°C. The samples were kept at the reaction temperature for 2 hours before they were cooled at 200°C/h down to room temperature.

3.5 Sample analyses

3.5.1 SEM

Some selected powder samples were analyzed in a Hitachi SU6600 FESEM. The powder was sprinkled onto a carbon tape and was also coated with carbon. This was done in order to minimize the charging effect which is often seen in poorly conducting samples. Silicon conducts electricity fairly well, but SiO_2 is a poor conductor and Si_3N_4 is even worse.

A few samples were also investigated using the Quantax EDS from Bruker on the same Hitachi SEM.

3.5.2 XRD

A D8Focus equipped with a LynxEye PSD (Position Sensitive Detector) was used for the XRD analysis. Measurements were made in θ/θ mode from 10° to 80° 2θ. The 2θ step size was 0.01571° and the exposition time for each point was 0.25 sec. The slit was 0.2 mm wide.

The amount of α and β phases were calculated using the Topas program.

Chapter 4

Results

The aim of this chapter is to give an overview of the results obtained in this work and will be discussed in the next chapter. This work has in many ways been a mapping of the initial nitridation of silicon powders prepared in different ways. Due to the nature of the work there is a lot of data to present and much of it is of similar nature. The results have therefore been categorized after the treatment received by the silicon powder prior to nitridation, i.e., after the four branches in figure 3.2.1. In appendix C all the data are gathered in a few large tables instead of the divided tables presented in this chapter.

4.1 Powder characterization

The surface area of the powders were found using the BET-method. The surface area of powder A is 0.8330 m^2/g and the surface area of powder B is 1.0597 m^2/g. The 5-point BET surface area plot can be found in appendix A. The particle size distribution of powder A and B is shown in figure 4.1.1 and 4.1.2. The cut-off values for the powders are shown in table 4.1.1.

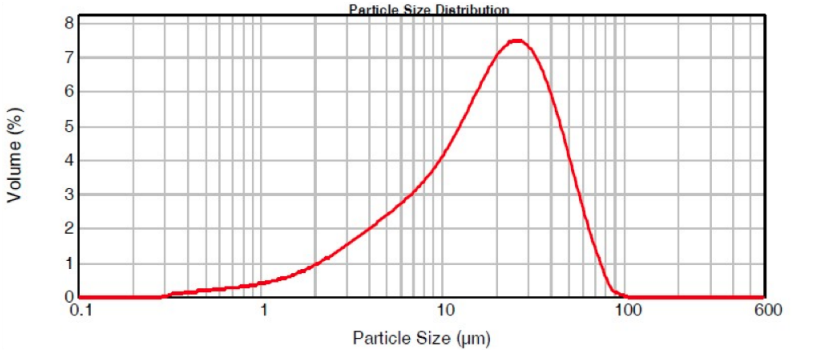

Figure 4.1.1: Particle size distribution of the silicon powder referred to as "Batch A." The measurements have been performed by Elkem.

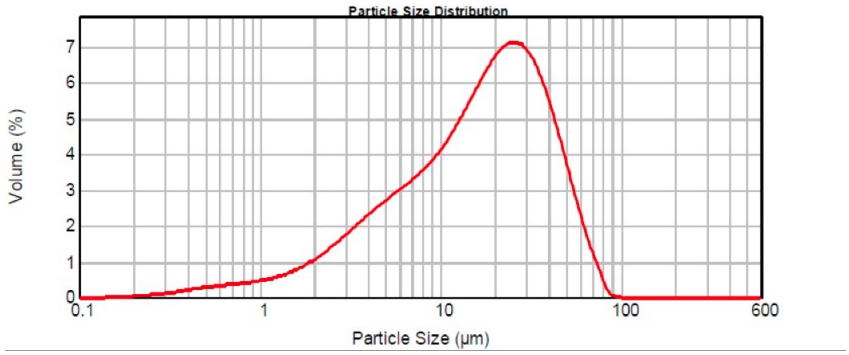

Figure 4.1.2: Particle size distribution of the silicon powder referred to as "Batch B." The measurements have been performed by Elkem.

Table 4.1.1: Cut-off values for the silicon powder provided by Elkem.

Sample (Ref. name)	*d(0.1) [µm]*	*d(0.5) [µm]*	*d(0.9) [µm]*
Batch A	3.739	18.626	45.475
Batch B	3.132	17.139	43.693

4.2 Nitridation of as-received silicon powder

Table 4.2.1 shows the weight increase based on weight measures before and after each nitridation. The table includes both TGA nitridation and large scale nitridations. As mentioned in section 3.4.1 a new set-up for the TGA was necessary. The samples nitrided with this set-up are marked with * after the sample name. The table shows that these samples seem to have a higher weight increase than the rest. It can also be seen that out of the two similar samples A-AR-L.1 and A-AR-L.2, the one with the highest initial weight has the lowest total weight increase.

Table 4.2.1: TGA and large scale nitridations of silicon powders in as received condition.

Sample code	*Storage condition*	*Init. Weight [mg]*	*Weight increase [%]*
A-AR-S.1	Dry (exicator)	19.29	5.90
A-AR-S.2		20.25	4.35
A-AR-S.3*		31.32	7.50
A-AR-L.1	Dry (exicator)	359.0	3.79
A-AR-L.2		950.7	3.19
B-AR-S.1	Dry (exicator)	21.64	2.68
B-AR-S.2*		36.65	4.47

Figure 4.2.1 shows the mass increase curves from the TGA. No nitridation is expected to occur before 1150°C. All the curves have been fitted so they start from zero at 1100°C. This was necessary because there is always some instability with regards to background noise, e.g. gas expansion, upon heating. This meant that at 1100°C the samples could be scattered as much as ± 0.7%, which would have made it difficult to compare the results. Also, it is the trends that are important, not the end weight increase. The final mass increase showed in the curves differ from the measured weight increase showed in table 4.2.1 and is related to the TGA troubles mentioned in experimental. The measured weight increase from the table is therefore more correct, while the TGA curves show the trends of the nitridation reaction.

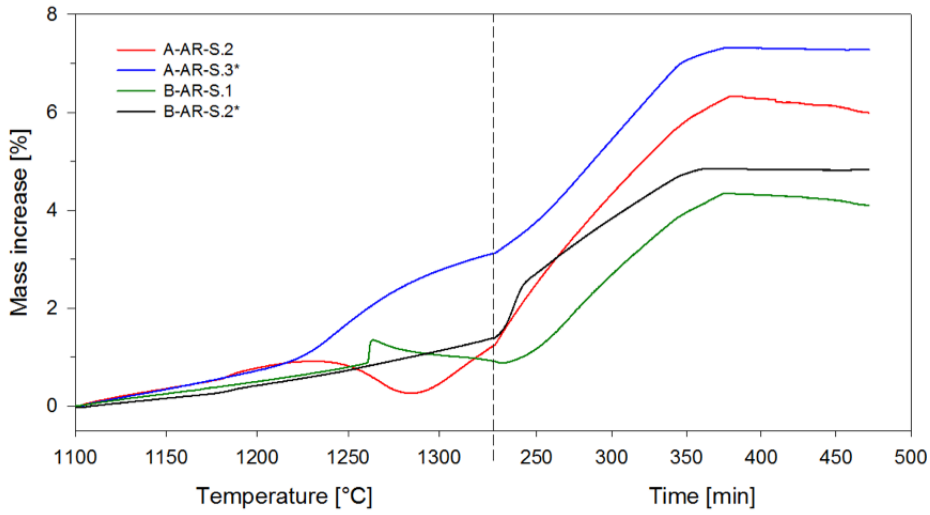

Figure 4.2.1: TGA nitridation of as received silicon powder. The samples were heated at 10°C/min to 1100°C, where the heating rate was slowed to 2°C/min. The samples were kept at 1330°C for 2 hours before cooling at 10°C/min to room temperature. The 50/50 N_2/Ar gas mixture was admitted at 40 mL/min (60 mL/min for DTA set-up) the whole time. The samples nitrided with the DTA set-up show different trends compared to similar samples nitrided with DSC set-up.

The first part of the x-axis shows the slow heating of the sample from 1100°C to 1330°C. The second part shows the 2 hour long isothermal step at 1330°C and the cooling to room temperature. Note that the time depicted is the time from the experiment started. The isothermal step starts at 222 minutes and ends after 342 minutes. As can be seen, there is still some weight increase as the temperature drops, which is why also the cooling step is shown in the figures

It can be seen that there are some noteworthy differences in the nitridation due to the different TGA set-up. Sample A-AR-S.2 was nitrided with the DSC set-up and it can be seen that the sample experiences a weight reduction around 1250-1300°C. This weight drop is not seen in A-AR-S.3* which is essentially the same sample only it was nitrided with the DTA set-up. For the DSC nitrided sample B-AR-S.1, a similar weight reduction can be seen, but there is also a rapid weight increase just before the weight reduction. These trends are not observed in the DTA nitrided sample B-AR-S.2*.

4.2.1 XRD analyses

The purpose of this section is to present an overview of the degree of nitridation and the different amounts of α -and β-Si_3N_4 in the nitrided samples. This is best done quantitatively by using a purposely designed program (such as Topas) which calculates the amount of each phase present, but it can also be done qualitatively just by viewing the diffractograms. For the next sections only the quantitative data will be presented (all the

diffractograms can be found in appendix B), but for this section the diffractograms will also be presented.

Figure 4.2.2 shows the diffractograms for the samples from figure 4.2.1. Because these are two different powders it is actually not that hard to see there are differences in the diffractograms, which is one reason this figure was chosen to be presented. Another reason is to show the reader that some of the indicated phases are barely more than background noise. This makes the calculations done in Topas less accurate and should be kept in mind.

For the samples from batch A the α peaks seems to be higher than in the samples from batch B. Similarly, β peaks are less intense in batch A samples than i batch B samples. Sample B-AR-S.1 shows a peak for SiO_2, which is not seen in any of the other diffractograms. The high peak at around 28° is the peak for silicon. As mentioned in section 3.5.2, the XRD scan was done from 10° to 80° 2θ. The full scan range was used to calculate the amount of each phase present, however, after 45° there is little α and β phases. It should also be noted that the phase composition was calculated based on the assumption that the only crystalline phases present were silicon and α -and β-Si_3N_4. As can be seen from the diffractograms in appendix B this is not a bad assumption as SiO_2 is only present in two other samples.

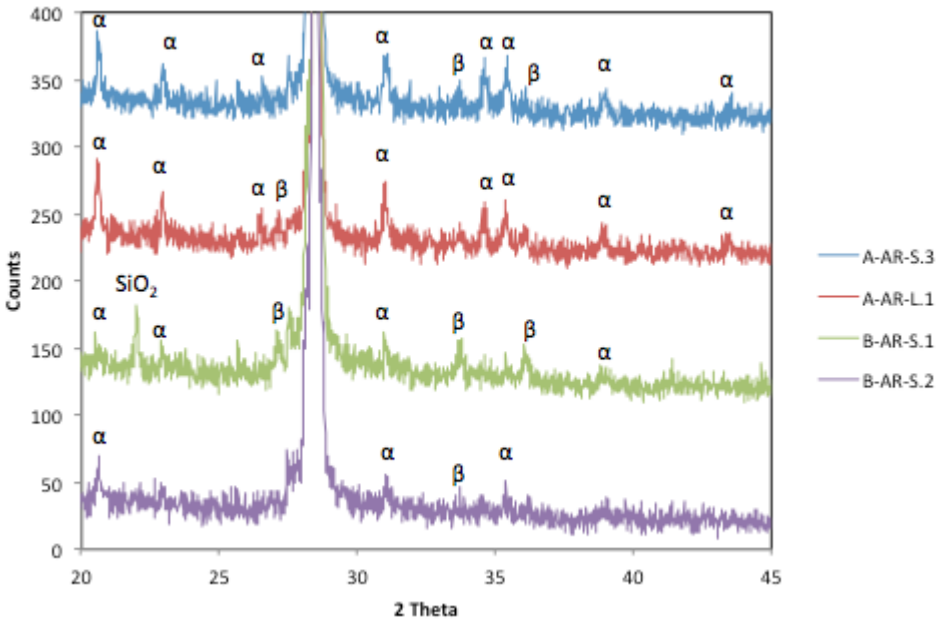

Figure 4.2.2: Diffractogram of large scale and TGA nitrided samples from batch A and batch B. There is a difference in the two powders in the amount of α-Si_3N_4 phase present. B-AR-S.1 also stands out with some crystalline SiO_2. Note that some of the peaks are barely higher than the background noise.

The degree of nitridation for the as received samples are shown in table 4.2.2. Sample A-AR-L.1 has been more converted than sample A-AR-L.2 which was the bigger sample size. B-AR-S.1 also stands out with a very low α/β-ratio.

Table 4.2.2: Degree of conversion and amount of α- and β-Si_3N_4 in samples nitrided in as received condition.

Sample	*Converted Si [%]*	*α [%]*	*β [%]*	*α/β-ratio*
A-AR-S.3*	11.1	10.0	1.1	0.90
A-AR-L.1	14.9	12.5	2.4	0.84
A-AR-L.2	10.9	8.4	2.6	0.77
B-AR-S.1	3.3	0.9	2.4	0.27
B-AR-S.2*	2.3	1.8	0.5	0.79

4.2.2 SEM analyses

Figure 4.2.3 shows differences in pure un-nitrided silicon particles and the sample A-AR-L.1. The pure silicon is characterized by a smooth surface and clear edges, while the surface on the nitrided sample is covered by a whisker (needle like) growth.

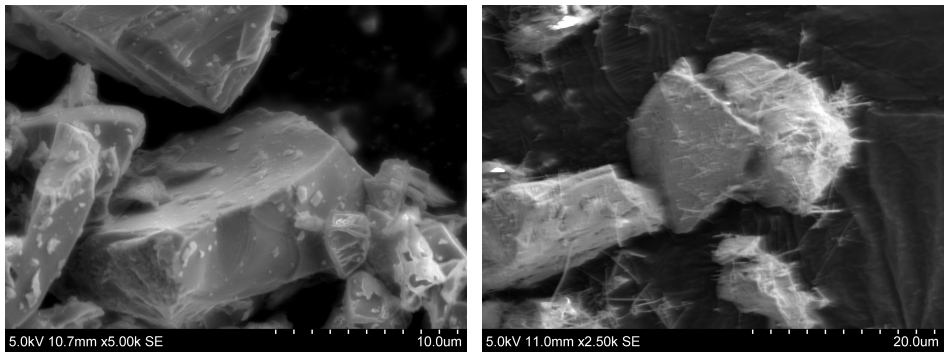

(a) **(b)**

Figure 4.2.3: Overview of the different morphologies in **a**) pure un-nitrided silicon and **b**) "as received" nitrided silicon powder (sample A-AR-L.1). A growth of some sort is visible on the nitrided sample.

4.3 Nitridation of silicon powders from humid storage

4.3.1 10°C humid storage

Table 4.3.1 shows the storage time and measured weight increase for the samples stored at 10°C and humid atmosphere prior to nitridation. Both the TGA and the large scale

nitridation seem to follow a trend where the total weight increase increases with storage time. Note that A-10D.36-S.1* has been nitrided with the DTA set-up.

Table 4.3.1: TGA and large scale nitridations of silicon powders after 10°C humid storage.

Sample code	*Storage condition*	*Days stored*	*Init. Weight [mg]*	*Weight increase [%]*
A-10D.1-S.1		1	18.76	4.20
A-10D.2-S.1	10°C - humid	2	22.84	4.25
A-10D.4-S.1	0.012 atm	4	19.63	3.97
A-10D.36-S.1*		36	34.62	6.67
A-10D.1-L.1	10°C-humid	1	293.1	4.84
A-10D.4-L.1	0.012 atm	4	301.6	5.97
A-10D.35-L.1		33	276.2	6.66

The TGA nitrided samples from table 4.3.1 are shown in figure 4.3.1. A-10D.36-S.1* stands out as it was nitrided with the DTA set-up. Otherwise the rest of the samples show very similar trends with a slight weight increase around 1210°C and a following weight reduction starting around 1260°C.

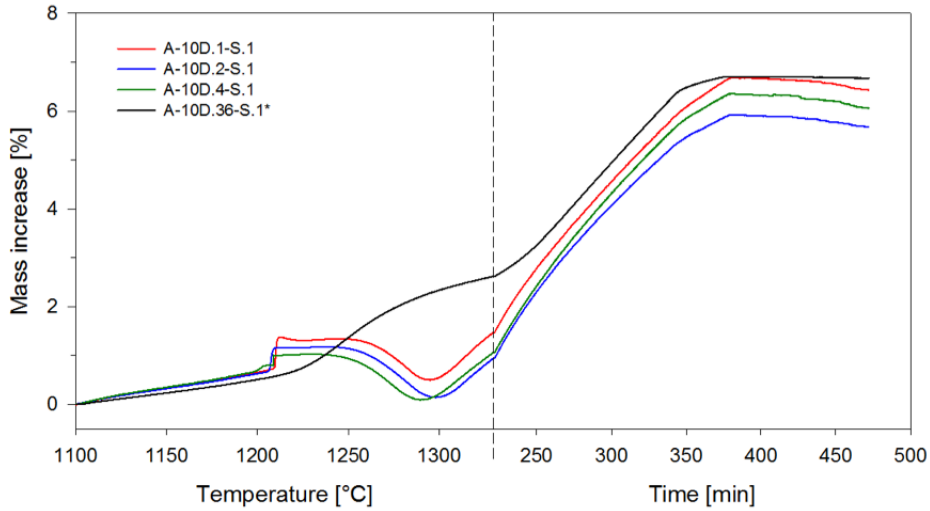

Figure 4.3.1: TGA nitridation of 10°C humid stored silicon powder. The heating program is the same as for figure 4.2.1 and the one shown in section 3.4.1. Apart from sample A-10D.36-S.1*, all the samples show a rapid weight increase at 1210°C and a weight reduction starting at 1260°C.

XRD analyses

Table 4.3.2 shows the amount of converted silicon for the 10°C humid stored samples. For both the large scale and TGA nitridation the amount of converted silicon increases with increased storage time. The large scale nitridation also shows a trend where the α/β-ratio increases with increasing storage time. These trends have been schematically shown in appendix D.

Table 4.3.2: Degree of conversion and amount of α- and β-Si_3N_4 in samples stored in 10°C humid atmosphere.

Sample	*Converted Si [%]*	*α [%]*	*β [%]*	*α/β-ratio*
A-10D.1-S.1	7.8	6.4	1.4	0.82
A-10D.2-S.1	9.5	7.3	2.2	0.77
A-10D.4-S.1	9.8	7.2	2.6	0.73
A-10D.36-S.1*	14.1	11.7	2.4	0.83
A-10D.1-L.1	14.6	11.3	3.3	0.77
A-10D.4-L.1	20.7	16.3	4.4	0.79
A-10D.35-L.1	22.9	18.6	4.3	0.81

4.3.2 22°C humid storage

The silicon powder that were stored at 22°C in humid atmosphere prior to nitridation is shown in table 4.3.3. Of the TGA nitrided samples, A-22D.4-S.1 stands out with very little weight increase compared to the two others. The section showing the large scale nitridations is a bit difficult to follow because of samples A-22D.1-L.1 and A-22D.2-L.1. These samples differ from the rest because of their high initial weight. They were larger in order to investigate differences in samples with a smaller surface are compared to the bulk sample. It can be seen from the table that these samples have gained a smaller total weight increase than the similar smaller samples.

Table 4.3.3: TGA and large scale nitridations of silicon powders after 22°C humid storage.

Sample code	*Storage condition*	*Days stored*	*Init. Weight [mg]*	*Weight increase [%]*
A-22D.1-S.1	22°C - humid	1	21.49	4.70
A-22D.4-S.1	0.026 atm	4	17.51	2.97
A-22D.36-S.1*		36	34.61	7.74
A-22D.1-L.1		1	990	4.38
A-22D.1-L.2		1	241.1	5.43
A-22D.2-L.1	22°C-humid	2	886.8	3.95
A-22D.2-L.2	0.026 atm	2	237.8	5.05
A-22D.4-L.1		4	301.1	5.21
A-22D.34-L.1		34	252.2	6.46

The TGA curves in figure 4.3.2 shows that A-22D.1-S.1 and A-22D.4-S.1 have similar trends with weight increase and weight reduction. The weight increase happens a little sooner and is a little smaller for A-22D.4-S.1, but the weight reduction seems to happen at the same temperature, approximately 1270°C. For the DTA nitrided A-22D.36-S.1* there is an increase in the weight just as the other samples have a weight reduction.

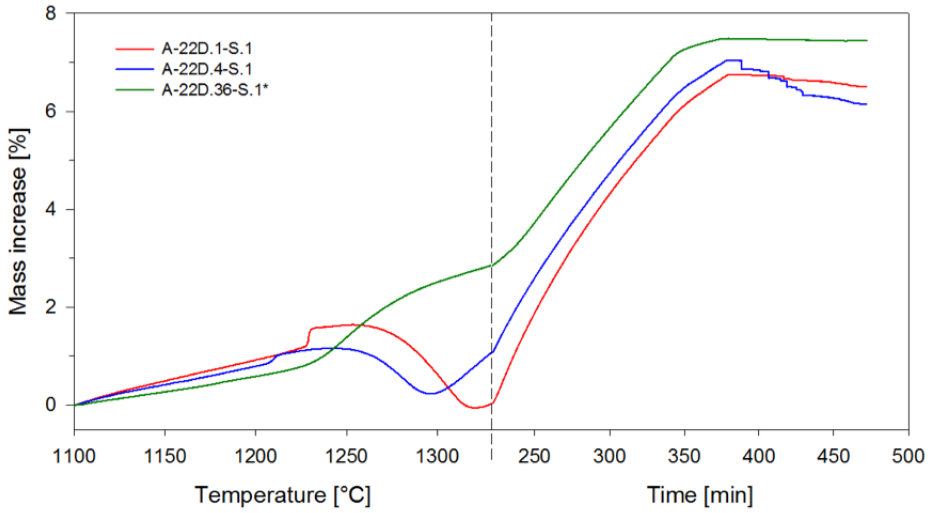

Figure 4.3.2: TGA nitridation of 22°C humid stored silicon powder. The DSC nitrided samples show a slightly, though rapid, weight increase before there is a large weight reduction. A-22D.36-S.1* has a slight weight increase when the other samples lose weight.

XRD analyses

The amount of converted silicon for all the 22°C stored samples are given in table 4.3.4. An increase in α/β-ratio after longer storage time can be seen for both the different nitridation furnaces. A-22D.4-S.1 stands out with very little converted silicon compared to the samples in the same series. The large scale nitridations show a trend where the amount of converted silicon increases as the storage time increases. Remember from table 4.3.3 that A-22D.1-L.1 and A-22D.2-L.1 had a much higher initial weight and must therefore be excluded from the trend. As with the samples stored at 10°C a graphical overview of these trends have been given in appendix D.

Table 4.3.4: Degree of conversion and amount of α- and β-Si_3N_4 in samples stored in 22°C humid atmosphere.

Sample	*Converted Si [%]*	*α [%]*	*β [%]*	*α/β-ratio*
A-22D.1-S.1	11.5	8.4	3.1	0.73
A-22D.4-S.1	7.6	5.9	1.6	0.79
A-22D.36-S.1*	10.8	9.0	1.7	0.84
A-22D.1-L.1	14.4	10.9	3.5	0.76
A-22D.1-L.2	15.3	11.2	4.1	0.73
A-22D.2-L.1	12.1	9.6	2.5	0.79
A-22D.2-L.2	16.4	13.1	3.3	0.80
A-22D.4-L.1	16.1	12.4	3.7	0.77
A-22D.34-L.1	17.4	14.2	3.2	0.81

4.3.3 SEM analyses

The samples that were stored under the same conditions, but at different lengths, showed few visible differences in the SEM. Figure 4.3.3 therefore shows samples A-10D.33-L.1 and A-22D.34-L.1 which have been stored at different conditions and for longer times than the rest of the samples, to evaluate the effect of the storage conditions. A-10D.33-L.1 (**a**, **c**) does not seem to have as much whisker growth (needle like structure) as the 22°C sample. But it seems, however, to be slightly rounder around the edges which could indicate that the 10°C sample has a thicker growth on the surface.

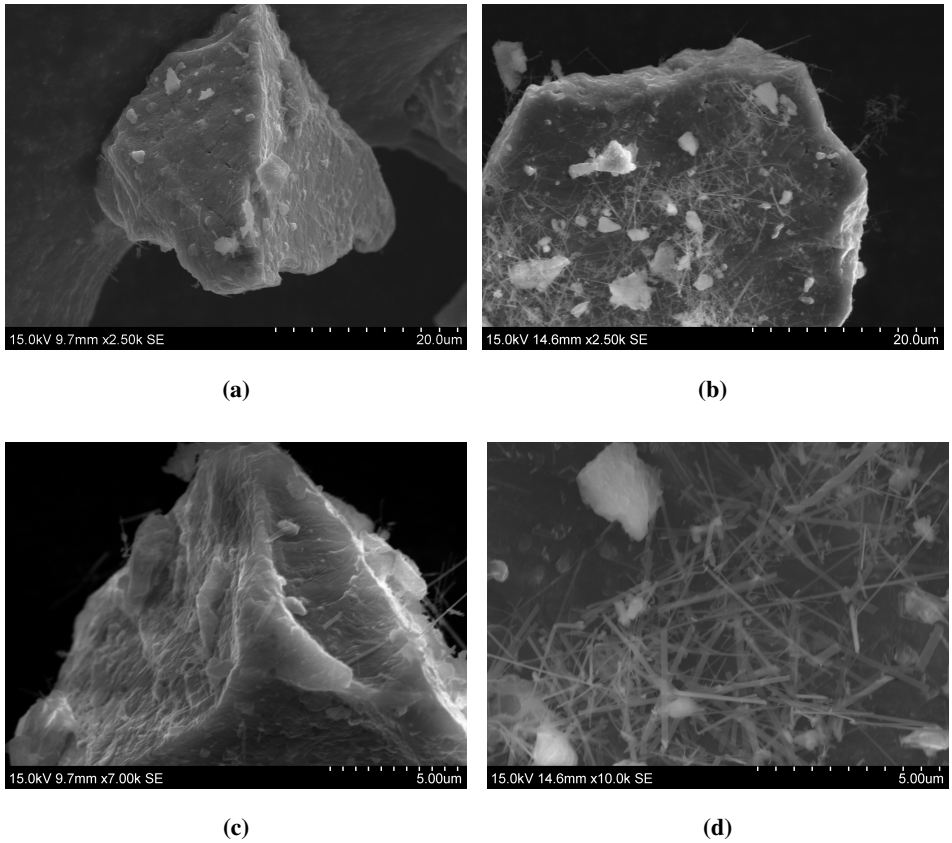

Figure 4.3.3: The figure compares sample "A-10D.35-L.1" (**a**, **c**) to sample "A-22D.34-L.1" (**b**, **d**) at different magnifications. The sample stored at 22°C seems to have a more needle like growth compared to the sample stored at 10°C. Image **c**) shows that growth on the 10°C sample is more laterally along the surface of the silicon particle.

4.4 Nitridation of thermally reduced silicon powders

4.4.1 Powders reduced at 1200°C

The powders reduced at 1200°C had a weight loss of ~0.2% after the reduction process. This seemed to be a little light, so only one batch was made this way. Table 4.4.1 shows all the samples that were nitrided after this treatment. Note the large difference in the weight increase between A-H2-D.0-S.1 and A-H2-D.0-L.1. They are the exact same powder only one has been nitrided in the TGA and the other in the large scale furnace. A-H2-22D.30-S.2 stands out with a slightly lower weight increase than what could be expected. Otherwise there seems to be a decreased weight loss with increased storage time.

Table 4.4.1: TGA and large scale nitridations of silicon powders which were thermally reduced at 1200°C to remove the surface oxide layer.

Sample code	*Storage condition*	*Days stored*	*Init. Weight [mg]*	*Weight increase [%]*
A-H2-D.0-S.1	None	0	18.24	6.80
A-H2-D.0-L.1	None	0	832	2.10
A-H2-22D.1-S.1	22°C - humid	1	17.39	6.90
A-H2-22D.30-S.1	0.026 atm.	30	16.56	5.86
A-H2-22D.30-S.2		30	18.21	3.51
A-H2-22D.1-L.1	22°C - humid	1	846	1.91

The nitridation curves shown in figure 4.4.1 indicate a very similar nitridation trend for all the samples. There is a slight difference with A-H2-22D.30-S.1 which does not have the characteristic weight increase at ~1180°C.

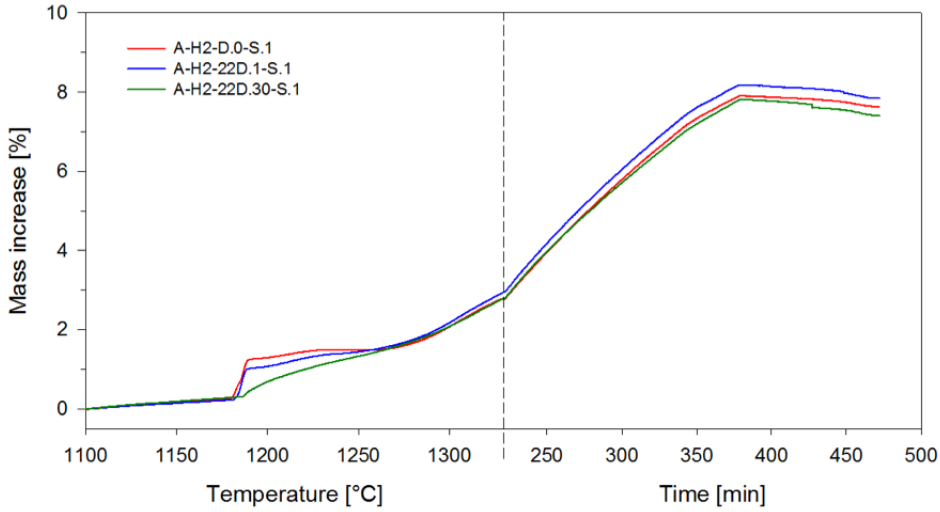

Figure 4.4.1: TGA nitridation of 1200°C thermally reduced humid stored silicon powder. Very similar trends for all the samples, the only difference is that A-H2-22D.30-S.1 does not have the characteristic weight increase at around 1180°C.

XRD analyses

Table 4.4.2 shows the amount of converted silicon for the 1200°C thermally reduced samples. The α/β-ratio is very similar for all the samples.

Table 4.4.2: Degree of conversion and amount of α- and β-Si_3N_4 in the samples that were thermally reduced at 1200°C.

Sample	*Converted Si [%]*	*α [%]*	*β [%]*	*α/β-ratio*
A-H2-D.0-S.1	9.0	7.4	1.6	0.82
A-H2-D.0-L.1	6.0	4.8	1.2	0.80
A-H2-22D.1-S.1	5.5	1.6	1.5	0.78
A-H2-22D.30-S.1	7.8	6.3	1.5	0.81
A-H2-22D.30-S.2	5.9	4.8	1.2	0.80
A-H2-22D.1-L.1	6.2	5.1	1.2	0.81

4.4.2 Powders reduced at 1300°C

For the 1300°C reduced powders the weight reduction was about 1%. The measured weight increase after nitridation for all the samples made this way is shown in table 4.4.3. The sample stored at 10°C after the reduction process has a lower weight increase after about 30 days storage time, whereas the sample stored at 22°C has a higher weight increase after increased storage time. There seems to be little differences in the weight increase between the two storage conditions. The powders from batch B still has a lower weight increase than similar powders from batch A.

Table 4.4.3: TGA and large scale nitridations of silicon powders which were thermally reduced at 1300°C to remove the surface oxide layer.

Sample code	*Storage condition*	*Days stored*	*Init. Weight [mg]*	*Weight increase [%]*
A-H2-D.0-L.2	None	0	257.5	2.14
A-H2-D.0-L.3		0	222.7	1.71
B-H2-D.0-S.1*		0	38.93	1.21
B-H2-D.0-L.1		0	188.3	0.69
A-H2-10D.1-S.2*	10°C - humid	1	32.68	5.08
A-H2-10D.32-S.1*	0.012 atm	32	35.30	4.53
A-H2-10D.32-L.1		32	308.2	2.34
A-H2-22D.1-S.2		1	18.89	5.24
A-H2-22D.2-S.1	22°C - humid	2	17.12	4.38
A-H2-22D.32-S.1*	0.026 atm	32	31.62	5.66
A-H2-22D.31-L.1		32	191.7	2.87

Figure 4.4.2 shows the nitridation curves for the samples stored at 10°C after being thermally reduced. Similar trends for both the curves, A-H2-10D.1-S.2 has a slightly higher mass increase rate.

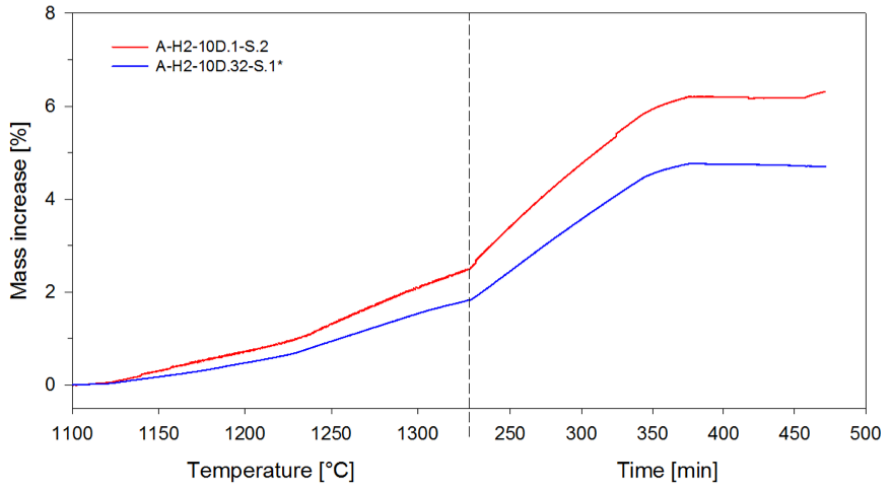

Figure 4.4.2: TGA nitridation of 10°C humid stored silicon powder after 1300°C thermal reduction. The weight increase starts early and A-H2-10D.1-S.2 seems to have a slightly higher mass increase rate. The trend is very similar for the two samples even though A-H2-10D.32-S.1 was nitrided with the DTA set-up.

Figure 4.4.3 shows the nitridation curves for the samples stored at 22°C after the thermal reduction. The trends are very similar, the nitridation rate seems slightly higher for A-H2-22D.1-S.1. The weight increase starts a little later than for the samples in figure 4.4.2.

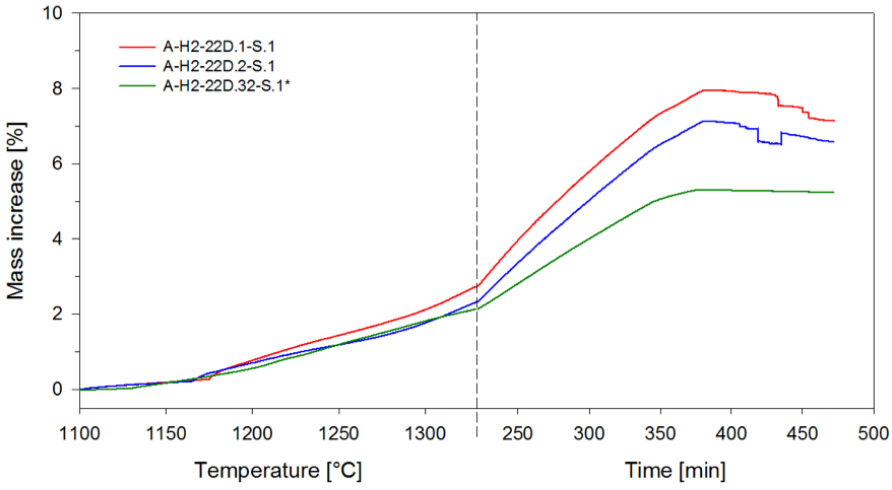

Figure 4.4.3: TGA nitridation of 22°C humid stored silicon powder after 1300°C thermal reduction. The weight increase seems to start at around 1170°C and all the samples follow a similar trend, even the DTA nitrided sample A-H2-22D.32-S.1*.

XRD analyses

The amount of converted silicon is showed in table 4.4.4. The powder from batch B immediately stands out with a very low amount of converted silicon and also a low *α/β*-ratio. A-H2-10D.32-S.1* has more converted silicon than A-H2-10D.1-S.2. That also goes for A-H2-10D.32-L.1 which has a higher conversion than A-H2-D.0-L.2 and A-H2-D.0-L.3. For the powders stored at 22°C the amount of converted silicon increases slightly with storage time, while the α/β-ratio drops.

Table 4.4.4: Degree of conversion and amount of α- and β-Si_3N_4 in samples that were thermally reduced at 1300°C before nitridation.

Sample	*Converted Si [%]*	*α [%]*	*β [%]*	*α/β-ratio*
A-H2-D.0-L.2	8.5	5.9	2.6	0.70
A-H2-D.0-L.3	9.4	7.7	1.7	0.82
B-H2-D.0-S.1	0.5	0.2	0.3	0.45
B-H2-D.0-L.1	2.3	1.3	1.1	0.54
A-H2-10D.1-S.2	5.6	4.2	1.4	0.75
A-H2-10D.32-S.1*	7.5	6.0	1.5	0.80
A-H2-10D.32-L.1	10.6	8.5	2.1	0.80
A-H2-22D.1-S.1	5.7	4.8	0.9	0.84
A-H2-22D.2-S.1	6.9	5.0	1.9	0.72
A-H2-22D.32-S.1*	5.9	4.2	1.7	0.71
A-H2-22D.31-L.1	8.5	6.7	1.9	0.78

4.4.3 SEM analyses

Figure 4.4.4 shows the difference in morphology in thermally reduced silicon particles before **a**) and after nitridation **b**). Before nitridation the particles are smooth and almost shiny, while they seem to be covered in "fur" after nitridation. Whisker growth can also be observed on the nitrided sample. It would also seem that the particles have attached to each other.

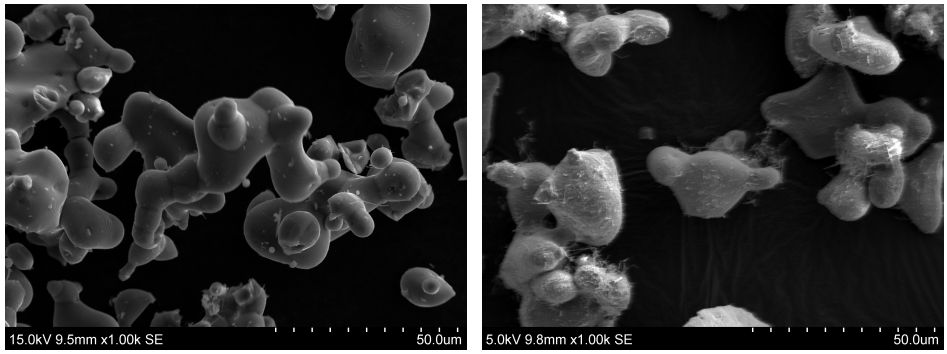

(a) **(b)**

Figure 4.4.4: The figure compares a sample reduced at 1300°C before nitridation (**a**) and after nitridation (**b**; sample "A-H2-D.0-L.3"). **a**) The surface of the particles seems rounded and smooth; **b**) The particles have the same morphology as in **a**), but the surface seems dimmer and appear to by covered by a growth of some kind. It can also be seen that the particles seem to have grown together.

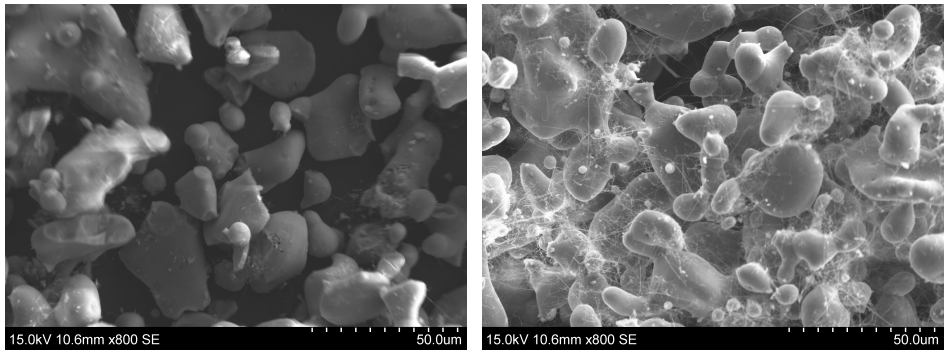

(a) **(b)**

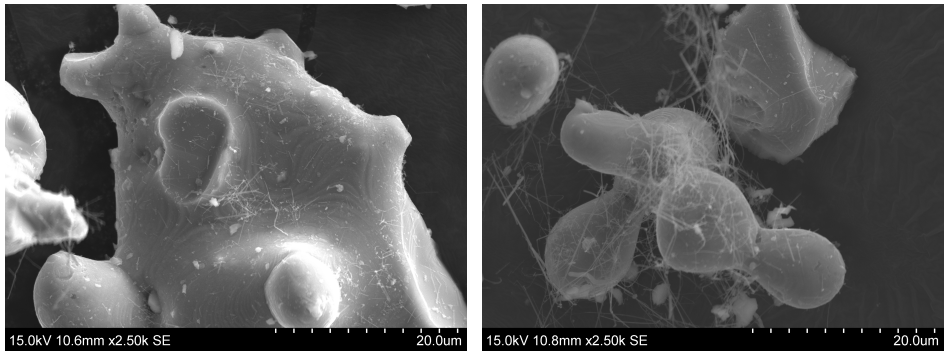

(c) **(d)**

Figure 4.4.5: The figure compares sample "A-H2-10D.32-S.1*" (**a**, **c**) and sample "A-H2-22D.32-S.1*" (**b**, **d**) at different magnifications. Both samples have a rounded particle morphology which seem to be covered by a thin layer of some sort. The sample stored at 22°C seems to have more whisker growth.

In figure 4.4.5 sample A-H2-10D.32-S.1* (**a**, **c**) and sample A-H2-22D.32- S.1* (**b**, **d**) are being compared. The first pictures shows a clear difference in the two samples. There is a lot more whisker growth on the sample stored at 22°C, although there is still some whisker growth on A-H2-10D.32-S.1* as well (figure 4.4.5c).

4.5 Nitridation of thermally oxidized silicon powders

After the thermal oxidation the sample had a weight increase of just over 1%. The weight increase after TGA and large scale nitridation is shown in the table below. There is a large difference in the weight increase between the two TGA nitrided samples although the sample is the same. The large scale results also stands out as it has a very low weight increase compared with the two other nitridations.

Table 4.5.1: TGA and large scale nitridations of silicon powders which were thermally oxidized at 900°C.

Sample code	*Init. Weight [mg]*	*Weight increase [%]*
A-TO-S.1*	44.44	3.58
A-TO-S.2*	36.47	7.98
A-TO-L.1	353.3	1.13

The nitridation curves in figure 4.5.1 shows the same difference between A-TO-S.1* and A-TO-S.2* as can be seen in the table above.

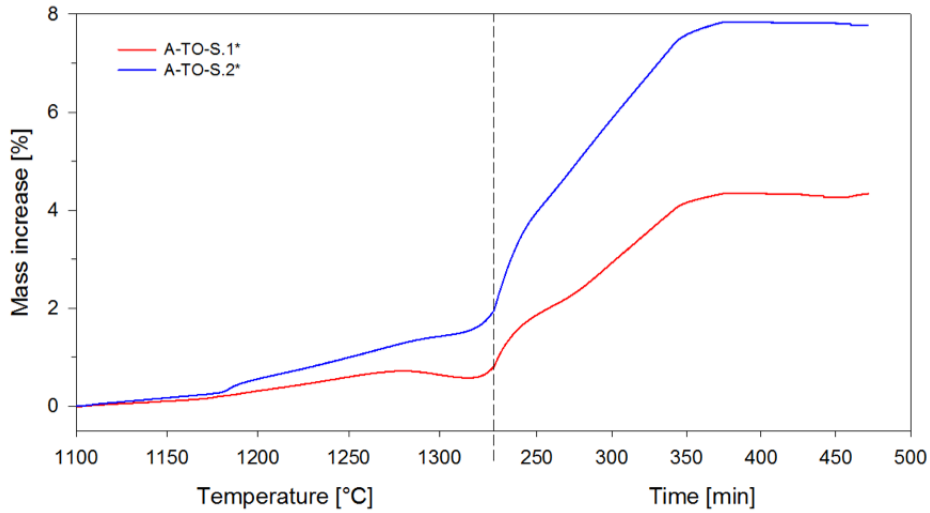

Figure 4.5.1: TGA nitridation of thermally oxidized silicon powder. Both samples are prepared the same way and nitrided with the DTA set-up, yet there is a large difference between the two curves. They also seem to have a slight weight loss just over 1300°C which have not been seen in any other DTA nitridations.

4.5.1 XRD analyses

The XRD analyses from the oxidized samples show a difference in converted silicon between the two TGA nitrided samples, and a good agreement between A-TO-S.2* and A-TO-L.1. The α/β-ratios are high and more similar than the amount of converted silicon.

Table 4.5.2: Amount of α- and β-Si_3N_4 in samples thermally oxidized before nitridation.

Sample	*Converted Si [%]*	*α [%]*	*β [%]*	*α/β-ratio*
A-TO-S.1*	10.6	9.2	1.2	0.89
A-TO-S.2*	16.3	14.4	1.9	0.88
A-TO-L.1	16.7	15.3	1.4	0.92

4.5.2 SEM analyses

After nitridation of the thermally oxidized samples, a white "cotton-ish" layer was visible on the inside of the crucible wall. This was especially inherent for sample A-TO-S.2*. The figure below show a picture of the sample A-TO-S.2* and the layer found on the crucible walls. An EDS analysis of this layer can be found in appendix E.

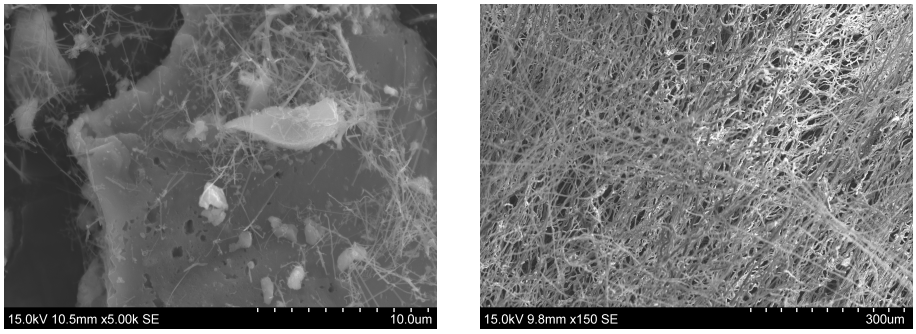

(a) **(b)**

Figure 4.5.2: The figure shows sample A-TO-S.2* (**a**) and the the white product found on the crucible walls after nitridation (**b**). There are clearly similarities between the growth on sample A-TO-S.2* and the product in **b**). Keep in mind that image **a**) is taken at a much higher magnification.

Chapter 5

Discussion

In this chapter the results presented in the preceding chapter will be discussed. However, for the results to be interpreted correctly, a few remarks regarding the nitriding conditions in the TGA and large scale furnace must be made. This includes differences in crucible geometry, gas flow and a few other functionalities. After these points have been made, the effect from the different storage conditions will be investigated. A comparison between the nitridation in the TGA and the large scale furnace will also be made.

All the data presented in the tables in the different sections in the results chapter are gathered in three large tables in appendix C if the reader wishes to look to these instead of shifting back an forth through the result chapter.

5.1 Important points regarding the nitriding conditions

The TGA apparatus has in many ways been the essence of this work and so a discussion of the properties and working details of the apparatus are important for the further discussion of the nitridation process. In a previous study by the author (Øvregård, 2012), the use of the TGA as a nitriding furnace was investigated. It was concluded that the precise weight logging and the ability to control the atmosphere made the TGA a very suitable nitriding furnace. The ability to evacuate the sample chamber and remove oxygen from the furnace is also a very important ability. As mentioned in section 2.4.2, it is important to keep a low oxygen partial pressure in order for a stable Si_3N_4 phase to form. The oxygen contaminations in the gas used was in the ppm range, giving an oxygen partial pressure of 10^{-5} atm which according to figure 2.4.1b is close to the limit for a stable Si_3N_4 phase to form.

Øvregård (2012) also found a suitable nitridation program for the TGA. Because of the exothermic nature of the Si/N_2 reaction a careful evaluation of nitriding atmosphere and

temperature is important to avoid "temperature run-off". The nitridation program used in this work is essentially the same, but the heating rate is slowed down at 1100°C instead of 1200°C. This was done after conferring with Arve Solheim who pointed out that there is a nitridation peak at around 1150°C which would be of importance when investigating the initiation of the silicon nitride reaction.

For the TGA nitridations it is also possible to do MS analyses which provides additional reaction information.

A problem with the TGA is that it requires very small samples. The risk of getting an inhomogeneous sample effect is therefore present. It should also be noted that the crucibles used are filled about one third with sample. Volatilization of the sample could create local atmospheres inside the crucible which differ from the admitted gas mixture.

The large scale furnace is a good counterpart to the TGA, as it allows for larger samples and uses open sample ships. It has also the possibility for a more dynamic gas flow (see figure 3.4.3). In the TGA, the atmosphere can get static because the gas is emitted from the bottom as seen in figure 3.4.1. A problem with the large scale furnace is that it cannot be evacuated before the measurement starts. In order to remove oxygen, the sample chamber was flushed with the reaction gas mixture before start. This should remove some of the oxygen, but it is probably a higher oxygen partial pressure in this furnace than in the TGA.

As mentioned in section 3.4.1 the Pt-element in the TGA broke some time into the experiments. To avoid this from happening again, the TGA set-up was changed from DSC to DTA. The difference is that for the DTA set-up the Pt-element is covered by the crucible and is in that way more protected. The DTA crucible is also much deeper than the DSC crucible.

Investigations of the damaged Pt-element showed that particles had condensed on the surface, thus impairing its conductivity. It is suspected that the particles are condensed SiO(g) from the silicon powder sample and could be related to the weight reduction shown in several of the nitriding curves at ~1300°C (a good example is figure 4.3.1). The partial pressure of SiO(g) has been calculated as a function of temperature for equation 2.12, which is the reaction for the Si/SiO_2 interface.

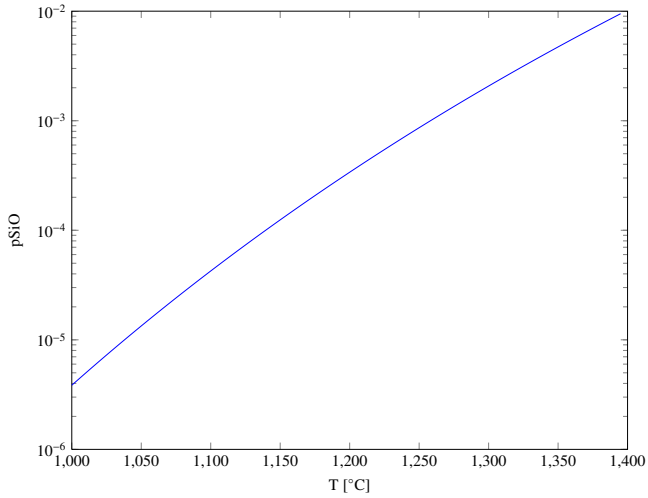

Figure 5.1.1: Calculated partial pressure of SiO(g) for the Si/SiO_2 interface reaction. As the the temperature reaches 1300°C, the partial pressure of SiO(g) is close to 10^{-3} atm. Thermodynamic data from Engh (1992).

At 1300°C the partial pressure of SiO(g) is around 10^{-3} atm which is quite large. It is therefore a good indication that the drop in the TGA mass increase curves are from loss of SiO(g).

Changing the TGA set-up from DSC to DTA had one very important effect on the nitridation process. The new crucible were much deeper than the last so that evaporating SiO(g) condensed on the crucible walls before it could escape the crucible. This was visible to the naked eye as a white cotton-ish cover on the sides of the crucible. For extra confirmation the "cotton" was studied with EDS (appendix E) which showed large peaks for oxygen and silicon. In figure 4.3.1 the effect of non-escaping SiO(g) can be seen for sample A-10D.36-S.1* compared to DSC nitrided samples. At the same time as the other curves drops, there is an increase in weight for the sample nitrided with the DTA set-up. The weight increase indicates that the nitridation reaction is in process, but for the other samples the mass loss due to SiO(g) is higher than the weight gained from the silicon nitride reaction, and so the net result is a weight loss.

The reader might have observed that the end, net, weight increase showed on the nitridation curves does not match the measured total weight increase shown in the tables. This is the case for the nitridations with the DSC set-up. The reason for this is that evaporated SiO(g) condensed on the Pt-element which registers the weight differences. Some of the loss from SiO(g) have therefore been registered by manual weighing, but not by the TGA apparatus because the sample has condensed on the weight. The DTA set-up gives a much more accurate result (This can be seen in figure 4.3.1 and table 4.3.1). This is both because the high crucible walls stops SiO(g) from leaving the crucible and because the gas flow was increased to make sure escaped SiO(g) was swept away before condensing.

Some samples were discarded after nitridation due to a net mass loss instead of mass increase (as expected from the nitridation reaction). These samples were characterized by a sudden drop in mass after only about half an hour. The mass drop was over 4% for some of the samples. The reason for mentioning this is that some of the nitrided samples which are included in the results might have suffered from this effect. Samples A-22D.4S.1 (figure 4.3.2) and A-H2-22D.30-S.2 (figure 4.4.1) show a lower weight increase than expected and were also characterized by a drop in the beginning of the experiment, though not nearly as large a drop as for the discarded samples. A graphic comparison of these samples with the discarded ones can be seen in appendix G. One explanation for this weight loss could be related to loss of humidity. Most of the discarded samples had been reduced with hydrogen and it is possible that they had accumulated a certain amount of humidity before they were nitrided. Some of these samples were run again with the MS connected to the TGA to investigate whether the weight loss was due to vaporization or just some artifact in the TGA. For some reason the data from the MS was never logged so the question is still unanswered.

5.2 Effects from storage conditions and pre-treatment on the nitridation reaction

This section will attempt to summarize some of the differences in degree of nitridation due to the various treatments before nitridation. Further, some of the most eminent phenomenons in the nitridation curves will be discussed and then a model to describe the results from the nitridation process and its variations will be presented.

Figure 5.2.1 shows the nitridation curves for the as received powder and the samples stored in humid atmospheres, both the thermally reduced and the ones that were stored in as received condition. For this comparison the samples with the longest storage time are used, as these are expected to show the largest differences. It is clear that the samples that were pre-treated before nitridation has a lower weight increase than the other samples. In addition they do not show the weight increase around 1250°C which the other samples show.

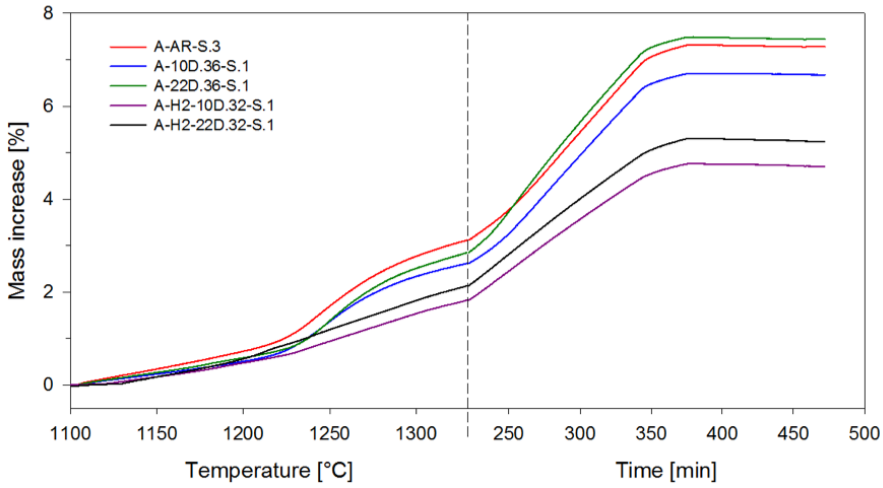

Figure 5.2.1: TGA nitridation of samples from humid storage, with and without thermal reduction and in as received condition. The thermally reduced samples stand out from the rest as they do not show the slight weight increase around 1250°C, seen in the other samples.

The obvious difference in the powders before the nitridation is the thickness of the surface oxide layer. In her work, Nymark (2012) showed that the oxide thickness on samples stored at 22°C was larger than on samples stored at 10°C. Thinking in these terms it would appear that the sample with the thinnest oxide layer (A-H2-10D.32-S.1*) has the lowest weight increase and oppositely the sample with the thickest oxide layer (A-22D.36-S.1*) has the largest weight increase. It should be noted that this is an expected oxide thickness, not a measured thickness. For this work the measuring of the oxide thickness was not done. Another remark should be made regarding the thermally reduced samples. As was shown in figure 4.4.4 there is a sintering effect on the pre-treated samples. This implies that these samples have a reduced surface area, which has a negative effect on the nitridation reaction (section 2.6.2). Much literature reports on doing similar pre-treatments to the one used in this work, although at a much shorter time interval, yet they still report on having removed all the surface oxide layer. It would seem that removing any residual oxygen is an important part of being able to efficiently remove the oxide layer. As mentioned, the large scale furnace used for the thermal reduction held no possibility to remove oxygen. If oxygen could be effectively removed it should be possible to remove the oxide layer in a shorter period of time and perhaps avoid the sintering effect. For the following discussion it will be assumed that the observed effects are due to the removal of the oxide layer and not the sintering effect

The results after humid storage and pre-treatment indicate that the bigger the oxide layer the larger the weight increase. Arguments could be made that sample A-AR-S.3* should have a lower oxide thickness than the sample stored at 10°C humid atmosphere, thus its weight increase should place it in-between the pre-treated and humid stored samples. Explanations could be that the as received sample actually has a lower oxide thickness than

the 10°C humid stored sample or that one of the samples could be subjected to inhomogeneous sample selection. Either way, there seems to be a connection between the weight increase and the oxide thickness. This is a surprising results because the literature is clear on the fact that the silicon surface oxide layer has a retarding effect on the nitridation reaction.

The weight increase by itself is not a very accurate measure of the degree of nitridation, although it gives a good indication. As mentioned in section 2.5.3, the conversion of silicon to silicon nitride follows a weight increase of 66.49%. This weight increase is seldom observed due to volatile species. The discussion above shows how SiO(g) escapes the crucible and therefore leads to a lower measured weight. The results from the TGA must therefore be compared with calculations of the degree of conversion from silicon based on the XRD results. For convenience the selected samples are shown in table 5.2.1.

Table 5.2.1: Degree of conversion and amount of α- and β-Si_3N_4 for the samples from figure 5.2.1

Sample	*Converted Si [%]*	*α [%]*	*β [%]*	*α/β-ratio*
A-AR-S.3*	11.1	10.0	1.1	0.90
A-10D.36-S.1*	14.1	11.7	2.4	0.83
A-22D.36-S.1*	10.8	9.0	1.7	0.84
A-H2-10D.32-S.1*	7.5	6.0	1.5	0.80
A-H2-22D.32-S.1*	5.9	4.2	1.7	0.71

The table shows that the samples that were thermally reduced prior to storage has indeed a lower conversion than the samples stored in humid atmospheres in as received condition. However, these results indicate that the samples stored at 10°C have been more converted to silicon nitride than the samples stored at 22°C. It therefore seems likely that there is some weight increase from another reaction in addition to the silicon nitride reaction. This is most likely due to the formation of SiO_2(s) from SiO(g) and O_2. As mentioned above, there are quite large weight losses in some curves due to loss of SiO(g). Under the assumption of a weight loss of 1% and using the density of amorphous SiO_2 it has been calculated that this weight loss corresponds to an oxide thickness of 3.71 nm (full calculation in appendix H). The resulting thickness is more than what is likely based on the thicknesses measured by Nymark (2012). It is therefore an indication that passive oxidation occurs, and since all the experiments in figure (ref tga diskusjon) is nitrided with the DTA set-up, most of the SiO(g) did not escape, but condensed inside the crucibles as SiO_2.

Before a more detailed description of the nitridation mechanism is proposed it is necessary to look at another phenomenon which occurs in some of the samples nitrided with the DSC set-up. Figure 4.3.1 shows a rapid weight increase at approximately 1210°C. It is likely that this weight increase is due to the formation of a silicon nitride layer on the bare silicon surface. If this is the case then, assuming an average weight increase of 0.5%, it can be calculated that the silicon nitride layer has to be 1.94 nm thick, which is a plausible thickness considering the short time it takes to create (full calculation in appendix I). Table 5.2.2 shows where the weight increase is located for different samples from batch

A.

Table 5.2.2: Temperature onset for the formation of Si_3N_4. The parenthesis in some of the sample names indicates the temperature for the thermal reduction.

Sample	*Temperature [°C]*	*Weight increase [%]*
A-10D.1/2/4	1210	~0.5
A-22D.1-S.1	1230	~0.3
A-22D.4-S.1	1210	~0.1
A-H2-22D.0/1 (1200)	1180	~0.9
A-H2-10D.1/32 (1300)	1130	close to nothing
A-H2-22D.1/2/32 (1300)	1170	close to nothing

The table shows that the samples with the estimated largest oxide layer thickness (stored at 22°C humid atmosphere) has the latest onset temperature for the silicon nitride formation. The earliest onset temperature (1130°C) are for the samples stored at 10°C humid atmosphere after thermal reduction at 1300°C, which is also the samples suspected to have the least oxide thickness.

In 2.5.1 it was pointed out that a very thin layer of silicon nitride formed on the silicon surface could inhibit further reaction, due to the very slow diffusion of species through the solid Si_3N_4 product. If the weight increase indicated in table 5.2.2 is attributed to the formation of this surface layer it could explain why the samples with a later onset has a higher degree of nitridation. However, if this is true, then the weight loss from SiO(g) must either be something else or the formation of the Si_3N_4 layer has occurred on the Si/SiO_2 via diffusion through the oxide layer. It seems unlikely that the mass loss could be from anything other than SiO(g), which means that the silicon nitride must form on the Si/SiO_2 interface. The formation of such a layer by diffusion through the oxide layer is possible as mentioned in section 2.5.3. But there is another problem with this theory. If the Si/N_2 reaction is inhibited due to slow diffusion in silicon nitride, then silicon nitride, cannot diffuse outwards and react with SiO_2 and give the registered weight loss from SiO(g). The following model is therefore proposed as a nitridation mechanism*:

*It is stressed that this is only a help for understanding the results from this investigation. The author does not mean to imply that the results gathered from this research is adequate enough to present a model for the nitridation mechanism.

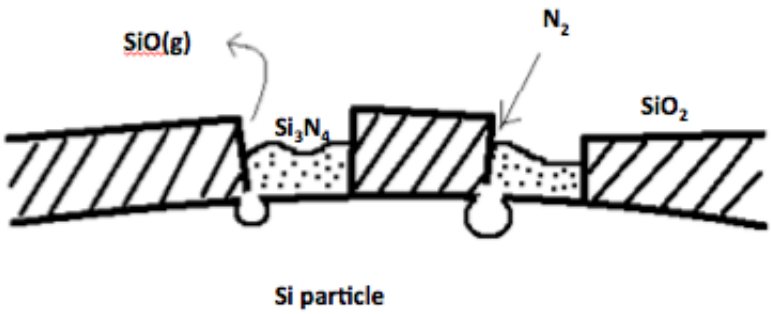

Figure 5.2.2: The figure shows a proposed model for the nitridation reaction, starting when bare silicon surface is exposed. The boundary between the oxide layer and the silicon nitride can provide easy diffusion paths for evaporating SiO(g) and incoming nitrogen. As SiO(g) is formed, the oxide layer is gradually removed and gives room for the silicon nitride reaction together with pores left behind from reacted silicon.

If the oxide layer is removed in pieces, i.e., reverse island growth, then the weight increase from the figures could be from silicon nitride formation on the patches with exposed silicon surface. This explanation allows active oxidation at the Si/SiO_2 interface which gives the observed weight reduction. As the evaporation of SiO(g) continues, more silicon surface is exposed for the silicon nitride reaction. The slope of the curves in the isothermal section has been calculated in appendix J and it showed that the highest growth rate was the thermally oxidized sample A-TO-S.2* which had a slope of 0.036%/min. The sample with the slowest growth rate was the thermally reduced and 10°C humid stored sample A-H2-10D.1-S.1 with a slope of 0.025%/min. The differences in growth rate between the samples are very low and could indicate that by the time the reaction temperature is reached, the silicon nitride film covers the entire surface and therefore only a slow reaction by diffusion is possible. The observation that none of the nitrided samples showed any sintering effect could also indicate that a silicon nitride layer has been formed before the highest temperatures are reached, because silicon nitride is very hard to sinter. The slightly higher reaction rate for A-TO-S.2* could be because the removal of the oxide layer (which is assumed to be thicker than for any other sample) disrupts the formation of the silicon nitride film, leaving it cracked and enhanced diffusion in these cracks is possible. But it could also be additional weight gain from condensing SiO(g).

The different onset temperatures for the initiation of the nitrogen reaction can be explained by the thickness of the oxide layer covering the surface. As general literature states, the nitridation reaction will not start before the oxide layer has been removed (except for a very thin layer which can form via diffusion). The thermally reduced samples will therefore have an early temperature onset for the nitridation reaction because there is little oxide to remove. In figure 4.4.2 it can be seen that there is no peak in the onset temperature and that the nitridation seems to proceed at a slow rate. Figure 4.3.2 shows the nitridation of the samples with assumed thickest oxide layer, and it can be seen that the onset temperature is much later than for the reduced samples. The observed weight increase before the peak can be explained by passive oxidation. As mentioned earlier, the weight loss from SiO(g)

needs more SiO_2 than what is likely to exist prior to nitridation. It can also be some nitridation by diffusion through the oxide layer.

The little peak in nitridation cannot be observed in samples nitrided with the DTA set-up. This could be because these samples had too much oxide layer or because the geometry of the DTA crucible did not allow much of the SiO(g) to escape. In order to remove the oxide layer, SiO(g) must be transported away to keep a low enough p_{SiO} for the reaction to continue. If the partial pressure of SiO(g) is high, the removal of the oxide layer is expected to go at a slower rate.

In section 4.4.1 the author expressed some concern regarding the samples reduced at 1200°C. The weight reduction was about 0.2% which seemed to be a little low. Table 5.2.2 shows that it takes longer time for the nitridation reaction to initiate for the 1200°C sample, than the ones reduced at 1300°C. This confirms the suspicion that the reduction at 1200°C did not sufficiently remove the oxide layer.

The results from the thermally oxidized samples are quite unexpected. In a previous work (Øvregård, 2012) nitrided a similar silicon powder after the same thermal oxidation program and the results showed close to no silicon nitride. One difference between the experiments are that the latest results were nitrided with the DTA set-up. Passive oxidation on crucible walls could explained the high weight increase. Looking at table 4.5.1 and comparing the TGA nitridations with the large scale nitridations it can be seen that the large scale nitridation has a much lower weight increase. However, table 4.5.2 shows that the degree of nitridation corresponds well with the TGA curves. The low weight increase from the large scale nitridation can be explained by escaping SiO(g), but the resulting degree of nitridation shown in table 4.5.2 seems indisputable. It would therefore seem that the oxide layer created by the thermal oxidation was not thick enough to hinder the reaction. Section 2.5.3 mentions that a thickness of ~1µm is needed for this purpose.

In the results it is mentioned that there is a trend of increased conversion with increased storage time for the samples stored at 10°C and 22°C directly. The graphical overview shown in appendix D also shows that the increase in conversion is slightly logarithmic. The observations agrees with the conclusion that the oxide layer has a positive effect on the initial nitridation reaction, however, the changes are very small and are based only on a few data samples.

5.3 Effect of gas phase reactions

As mentioned in section 2.6.2, the silicon nitride formed via gas phase reaction is usually the whiskery α-Si_3N_4. Figure 4.3.3 shows the different morphologies on samples stored at 10°C and 22°C humid atmosphere prior to nitridation. It is clear that the whisker growth is more eminent in the sample stored at 22°C. This is also the case for samples that were thermally reduced and then stored at the humid temperatures as figure 4.4.5 shows that sample A-H2-22D.32-S.1* has more whisker growth than sample A-H2-10D.32-S.1*. This can be explained by the assumption of more oxide growth on the 22°C stored samples and

α-Si_3N_4 formation via equation (ii) in section 2.5.4. Although the whiskers are an easy indicator for the silicon nitride reaction, they do not seem to account for much of the weight increase. XRD results (table 4.3.2 and 4.3.4) show that despite the extra whisker formation for the 22°C stored samples, the degree of converted silicon is higher for samples stored at 10°C. The α/β-ratio is still high, which indicates that α-Si_3N_4 also forms as the hexagonal platelets and prisms mentioned in section 2.6.2. A high α/β-ratio is according to the theory that silicon nitride in large part grows as the phase formed by the initial seeds. Heating through the lower temperature region, where α phase is dominant therefore gives a high α/β-ratio.

It was mentioned in the result section that a trend could be observed in the α/β-ratio for the samples that were humid stored without being thermally reduced. This trend is very vague and little more than speculation and is therefore placed in appendix D. It can be said however that the highest α/β-ratios comes from A-TO-L.1 (0.92), A-AR-S.3 (0.90), A-TO-S.1 (0.89) and A-TO-S.2 (0.88). This includes all the thermally oxidized samples, so it is clear that the oxide layer aids in the formation of α-Si_3N_4.

5.4 Differences in TGA and large scale nitridations

To summarize this far, a comparison of the samples with the longest storage time is presented below. The samples are arranged after degree of nitridation and weight increase after nitridation. The as received samples are also included.

Table 5.4.1: An arranged overview of degree of nitridation and weight increase after TGA nitridation.

Weight increase	*[%]*	*Converted Si*	*[%]*
A-22D.36-S.1*	7.74	A-10D.35-S.1*	14.1
A-AR-S.3*	7.50	A-AR-S.3*	11.1
A-10D.36-S.1*	6.67	A-22D.36-S.1*	10.8
A-H2-22D.32-S.1*	5.66	A-H2-10D.32-S.1*	7.5
A-H2-10D.32-S.1*	4.53	A-H2-22D.32-S.1*	5.9

Table 5.4.2: An arranged overview of degree of nitridation and weight increase after large scale nitridation nitridation.

Weight increase	*[%]*	*Converted Si*	*[%]*
A-10D.33-L.1	6.66	A-10D.33-L.1	22.9
A-22D.34-L.1	6.46	A-22D.34-L.1	17.4
A-AR-L.1	3.79	A-AR-L.1	14.9
A-H2-22D.31-L.1	2.87	A-H2-10D.32-L.1	10.6
A-H2-10D.32-L.1	2.34	A-H2-22D.31-L.1	8.5

The differences in table 5.4.1 was discussed in the section above and could be attributed

to SiO(g) condensation on the crucible. It is interesting to observe that the weight increase for the large scale nitridation (table 5.4.2) corresponds much better with the degree of nitridation. This makes sense because of the geometry and conditions in this furnace. The open sample ship allows for easier escape for the volatile species, in addition, it has a more dynamic gas flow. Therefore, very little SiO(g) is condensing on the sample ship.

The results for the large scale nitridations also fit the explanation that the native oxide layer hinders the formation of the protective film. There is a large difference in the amount of nitridation between the samples stored in as received condition and the ones that were pre-treated before storage. The as received sample is expected to have an oxide layer thickness in-between these and the resulting amount of converted silicon seems to agree with this.

It seems to be a consistent result that the samples stored at 10°C has a higher degree of nitridation than the ones stored at 22°C. This could be explained by a higher p_{SiO} when nitriding the 22°C stored samples, resulting in a slow removal of the oxide layer and less amount of conversion. It should also be noted that the low conversion for the thermally reduced samples could come from the sintering effect. This has not been discussed in this work because there was not time to remove the oxide layer by any other method. Research on "un-sintered" reduced silicon powder is therefore necessary for further discussion.

The difference in amount of converted silicon between the TGA and large scale nitridation could be due to a higher surface to bulk ratio for the large scale nitrided samples. These samples could also be more exposed to the gas mixture due to the geometry of the sample ships and the gas flow. Generally there seems to be good agreement between the TGA and large scale nitridation.

5.5 Differences in nitridation between batch A and B

The very pure silicon powder (batch B) has not been extensively studied in this work. It has only been nitrided in as received and a thermally reduced state, no humid storage was done. The purpose of this was to gain a reference in nitridation differences between the two silicon qualities, as a starting point for future work. Looking at table 4.2.1 it can be seen that the weight increase on sample B-AR-S.2* is significantly lower than sample A-AR-S.3*. The difference in amount of converted silicon shown in 4.2.2 is even bigger. B-AR-S.1 have a very low α/β-ratio compared to the samples from batch A. This is to be expected as the nitridation reaction largely depends on impurities in the silicon in order to initiate. A lack of these impurities pushes the initiation of the reaction to higher temperatures where β-Si_3N_4 is more dominant. The α/β-ratio for the DTA nitrided B-AR-S.2* sample does not agree with this observation. However, the assumed increased p_{SiO} in the DTA crucible enhances the formation of α-Si_3N_4 whiskers. It was concluded earlier in the discussion that the weight increase from the whiskers are not substantial, but for the pure silicon the overall conversion is so low that it becomes important. The thermally reduced silicon from batch B has an even lower conversion and data from table

4.4.4 confirms the low α/β-ratio in the pure silicon.

Chapter 6

Concluding remarks

Silicon nitride cannot form on the surface of the silicon particles before the oxide layer has been removed. The oxide layer is removed by the Si/SiO_2 interface reaction:

$$SiO_2(amorph.) + Si(s) \rightarrow 2SiO(g)$$

It is believed that the oxide layer is removed in patches, exposing the underlaying silicon for the nitridation reaction. Silicon nitride product forms as islands in-between the gradually disappearing oxide layer. When the oxide layer is completely removed, silicon nitride grows to cover the entire surface. The silicon nitride film will effectively hinder further reaction because the diffusion through the solid product is extremely slow.

There was a large difference in the degree of nitridation between the samples that were thermally reduced before the humid storage, and the samples that were stored directly. The thermally reduced samples are likely to have a thinner surface oxide layer than the samples stored directly. It is therefore believed that the oxide layer hinders the formation of the protective silicon nitride film and thus samples with the thickest oxide layer have a higher degree of nitridation.

Samples stored at 10°C had a higher degree of nitridation than samples stored at 22°C although the 22°C samples are expected to have a thicker oxide layer. An explanation could be that the oxide thickness on the 22°C samples are so thick that the removal rate is too slow for a substantial amount of Si_3N_4 to form.

Gas phase reactions, especially the evaporation of SiO(g), means that weight increases from the TGA curves does not completely agree with the amount of nitridation calculated using XRD results. TGA is still a very good way to analyze the nitridation reaction, but care should be taken not to immediately associate a large weight increase with a large degree of nitridation.

There was good agreement between the results obtained in the TGA and the large scale furnace, although the samples from the large scale furnace had a higher degree of conversion. This is probably due to a larger surface to bulk ratio in favor of the large scale samples.

Nitridation of the very pure silicon powder, denoted as batch B, highlighted how much the nitridation reaction is affected by impurities. The degree of nitridation in the pure silicon powder was very little compared to batch A. The α/β-ratio for batch A powder was close to 0.9 for almost every sample and closer to 0.5 for batch B.

Chapter 7

Further work

Removing the oxide layer on samples before nitridation is a very good starting point for studying effects on the nitridation reaction, whether its differences in the oxide layer or just different silicon qualities. Thermal reduction did remove the oxide layer, but it also had a sintering effect. The smaller surface area created from the sintering effect makes it difficult to separate and study the effect of the oxide layer. It is therefore recommended to remove the oxide layer in a way that does not encourage sintering. This could be done by effectively removing the residual oxygen in the reaction furnace, before the thermal reduction, thus reducing the reaction time drastically. Another possibility is to use HF acid to remove the oxide layer.

A longer thermal oxidation should be conducted to try to increase the thickness of the oxide layer enough for it to inhibit the silicon nitride reaction. A higher calcining temperature is also possible, but the sintering effect should be kept in mind.

It was mentioned in the discussion that some nitridation curves showed a large weight reduction after a very short time. This should be investigated by an MS analysis to check whether or not this was an artifact from the TGA. If the result show evidence of humid species it could indicate that hydroxyl groups attach to the silicon surface when stored in humid atmospheres.

The effect of the different storing conditions should be measured with XPS to better explain the observed results after nitridation.

References

, 1992. Netzsch STA 449C Jupiter Instruction manual.

, Memsnet.org.
URL http://www.memsnet.org/material/siliconnitridesi3n4film/

Albano, P., Scian, A., Pereira, E., 1991. Secondary phases in nitrided si powders. Materials letters 11 (8).

Albano, P., Scian, A., Pereira, E., 1993. Silic. Ind. 57 (11/12).

Atkinson, A., Moulsen, A. J., Roberts, E. W., July 1976. Nitridation of high-purity silicon. Journal of Materials Science 59.

Billy, M., 1959. Preparation and characterization of silicon nitride. Ann. Chim. (Paris) 4.

Blegen, K., 1975. Special Ceramics 6. British Ceramic Research Association.

Blegen, K., 1976. Equilibria and kinetics in the systems si-n, si-o-n and si-c-o-n. Ph.D. thesis, NTH.

Boyer, S. M., Moulson, A. J., 1978. A mechanism for the nitridation of fe-contaminated silicon. Journal of Materials Science 13, 1637–1646.

Brunauer, S., Emmett, P., Teller, E., 1938. Adsorption of gases in multimolecular layers. Journal of American Chemistry Society.

Campos-Loriz, Riley, F. L., 1978. Factors affecting the formation of the alpha and beta phases of silicon nitride. Journal of Materials Science.

Campos-Loriz, D., Howlett, S. P., Riley, F. L., Yusaf, F., 1979. Fluoride accelerated nitridation of silicon. Journal of Materials Science 14.

Campos-Loriz, D., Riley, F. L., 1976. Effect of silica on nitridation of silicon. Journal of Materials Science 11 (1).

Campos-Loriz, D., Riley, F. L., 1979. The effects of hydrogen on the nitridation of silicon. Journal of Materials Science 14.

Dalgleish, B. J., Jennings, H. M., Pratt, P., 1980. On the reaction of nitrogen with high purity single crystal silicon. Science of Ceramics 10.

Dalgleish, B. J., Pratt, P., 1973. The microstructure of reaction-bonded silicon nitride. Proceedings of the British Ceramic Society 22.

Dawson, W. M., Moulson, A. J., 1978. The combined effects of fe and h2 on the kinetics of silicon nitridation. Journal of Materials Science 13.

Dervisbegovich, H., Riley, F. L., 1981. The role of hydrogen in the nitridation of silicon powder compacts. Journal of Materials Science.

Einarsrud, M.-A., 2013. Personal communication.

Engh, T. A., 1992. Principles of Metal Refining. Oxford University Press.

Giridhar, R. V., Rose, K., 1988. Conditions for thermal nitridation of si in n2-o2 mixtures. J. Electrochem. Soc.: SOLID-STATE SCIENCE AND TECHNOLOGY.

Glemser, O., Beltz, K., Naumann, P., September 1957. Zur kenntnis des systems silicium-stickstoff. Zeitschrift für anorganische und allgemiene Chemie 291 (14), 51–66.

Gregory, O. J., Richman, M. H., 1982. Nitridation of high-purity single-crystal silicon. Metallography 15.

Guthrie, R. B., Riley, F. L., 1973. Proceedings of the British Ceramic Society 22.

Hardie, D., Jack, K. H., August 1957. Crystal structures of silicon nitride. Nature 180.

Hojo, J., Shoji, T., Kato, A., 1975. Denki Kagaku Oyobi Kogyo Butsuri Kagaku.

Jennings, H. M., 1983. On reactions between silicon and nitrogen. Journal of Materials Science 18 (4).

Jennings, H. M., Richman, M. H., 1975. The use of microscopy for determining the formation of beta silicon nitride. Proc. of the Electron Microscopy Society of Southern Africa.

Jones, B. F., Lindley, M. W., 1976. Reaction sintered silicon nitride. part 2. Journal of Materials Science 11.

Jørgensen, H. T. S., 2011. Oxidation of silicon in aqueous media. Master's thesis, NTNU, Trondheim.

Kijima, K., Shirasaki, S., 1976. Nitrogen self-diffusion in silicon nitride. Journal of Chemical Physics 65 (7).

Kooi, E., van Lierop, J. G., Apples, J. A., 1976. Formation of Silicon Nitride at a Si/SiO2 Interface during Local Oxidation of Silicon and during Heat Treatment of Oxidized Silicon. Vol. 123. The Electrochemical Society.

Kuwabara, A., Matsunaga, K., Tanaka, I., 2008. Lattice dynamics and thermodynamical properties of silicon nitride polymorphs. Physical Review 78.

Maalmi, M., Varma, A., Strieder, W. C., 1998. Reaction-bonded silicon nitride synthesis: experiments and model. Chemical Engineering Science 53 (4), 679–689.

Messier, D. R., 1977. The alpha/beta silicon nitride phase transformation. Army Materials and Mechanics Research Center Watertown Mass.

Messier, D. R., Riley, F. L., Brook, R. J., 1978. The alpha/beta silicon nitride phase transformation. Journal of Materials Science 13.

Morgan, P. E. D., 1980. Alpha-beta-si3n4 question. Journal of Materials Science 15 (3).

Moulson, A. J., 1979. Reaction-bonded silicon nitride: its formation and properties. Journal of Materials Science 14 (5), 1017–1051.

Myhre, B., 1989. Kinetics of the nitridation of silicon. Ph.D. thesis, NTH.

Nittler, L. R., Amari, S., Gao, X., Walker, R. M., Zinner, E., 1995. Silicon nitride from supernovae. The astrophysical journal.

Nymark, A. M., 2011. Oxidation of silicon powder in humid air. Tech. rep., NTNU.

Nymark, A. M., 2012. Oxidation of silicon powder in humid air. Master's thesis, NTNU.

Øvregård, H., 2012. Silicon for silicon nitride-based products. Tech. rep., NTNU.

Papirer, E. (Ed.), 2000. Adsorption on silica surfaces. Vol. 90 of Surfactant Science Series. Marcel Dekker, Inc.

Parr, N. L., Martin, G. F., May, E. R. W., 1960. Preparation, microstructure, and mechanical properties of silicon nitride. In: Popper, P. (Ed.), Special Ceramics. Academic Press, New York, pp. 102–135.

Pavarajan, V., 2002. Roles of gas and solid components in the direct nitridation of silicon. Ph.D. thesis.

Pehlke, R. D., Elliot, J. F., 1959. Aime. Trans. Met. Soc. 215.

Pigeon, R. G., Varma, A., 1992. Some chemical reaction engineering considerations in the synthesis of silicon nitride. Chemical Engineering Science 47 (9-11), 2585–2590.

Pigeon, R. G., Varma, A., Miller, A. E., 1993. Some factors influencing the formation of reaction-bonded silicon nitride. Journal of Materials Science 28.

Popper, P., Ruddlesden, S. N., 1961. The preparation, properties, and structure of silicon nitride. Transactions British Ceramic Society 56.

Rahaman, M. N., Moulson, A. J., 1984. The removal of surface silica and its effect on the nitridation of high-purity silicon. Journal of Materials Science.

Riley, F. L. (Ed.), 1983. Progress in nitrogen ceramics. NATO ASI series E, Applied sciences; no. 65. NATO Advanced Study Institute on Nitrogen Ceramics.

Riley, F. L., 1989. Materials Science Forum.

Riley, F. L., 2000. Silicon nitride and related materials. Journal of American Ceramic Societym 83 (2), 245–265.

Rong, H. M., 1992. Silicon for the direct process to methylchlorosilanes. Ph.D. thesis, NTNU, Trondheim.

Ruddlesden, S., Popper, P., January 1958. The compound sr3ti2o7 and its structure. Acta Crystallographica 11 (1).

Sangster, R. C., 2005. Formation of Silicon Nitride. A California Canyon.

Shaw, N. J., Zelesnik, F. J., 1982. Journal of American Ceramic Society.

Solheim, A., 2013. Personal communication.

Somiya, S., Aldinger, F., Spriggs, R. M., Uchino, K., Koumoto, K., Kaneno, M. (Eds.), 2003. Handbook of advanced ceramics. Vol. 2. Academic Press.

Svanem, J. P., 2013. Personal communication.

Thompson, D. S., Pratt, P., 1967. The structure of silicon nitride. Science of Ceramics 3, 33–51.

Wang, C. M., Pan, X., Rühle, M., Riley, F. L., Mitomo, M., October 1996. Silicon nitride crystal structure and observations of lattice defects. Journal of Materials Science 31 (20), 5281–5298.

Wiik, K., 2013. Personal meeting.

Zerr, A., Miehe, G., Serghiou, G., Schwarz, M., Kroke, E., 1999. Synthesis of cubic silicon nitride. Nature 400.

Ziegler, G., Heinrich, J., Wotting, G., 1987. Relationships between processing, microstructure and properties of dense and reaction-bonded silcon nitride. Journal of Materials Science 22 (9).

Appendices

A BET surface area plots

The following two figures show the BET surface area plots for the powders from batch A and B respectively.

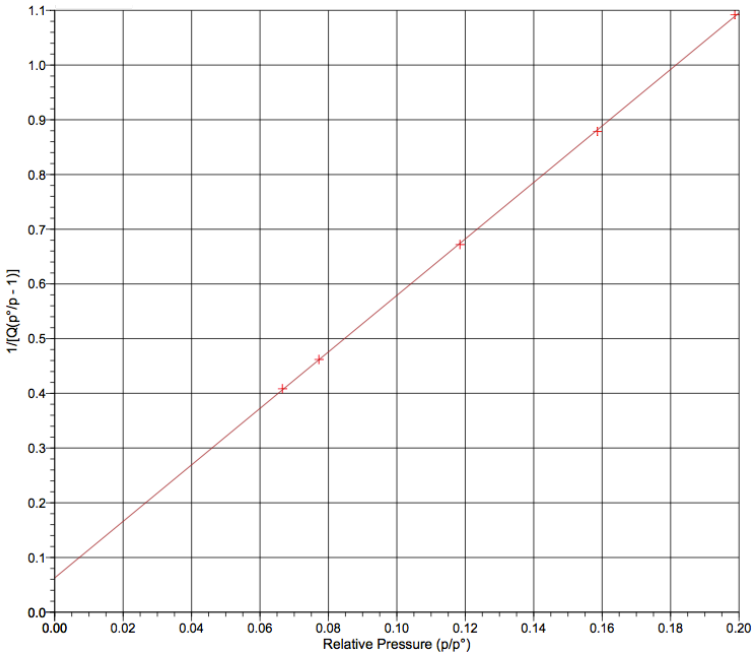

Figure A.1: BET surface area plot for the silicon powder from batch A. Degas temperature was 250°C.

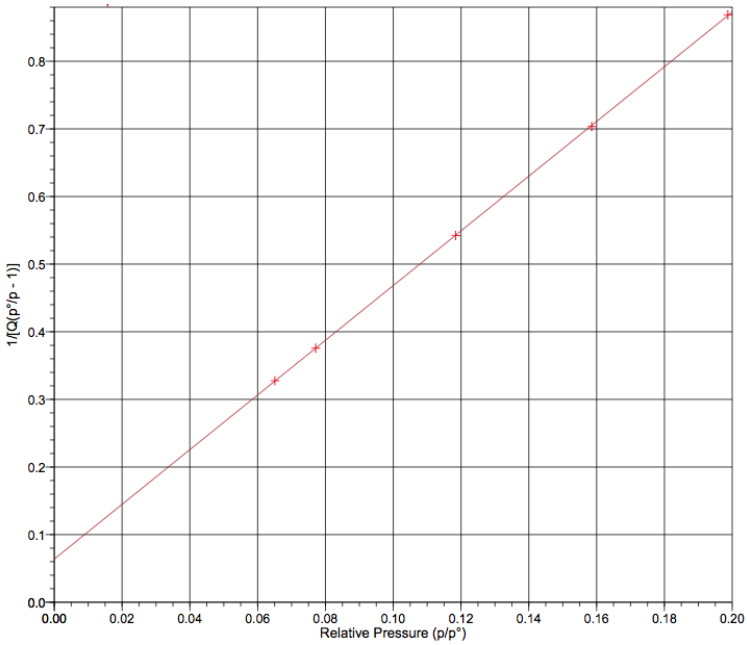

Figure A.2: BET surface area plot for the silicon powder from batch B. Degas temperature was 250°C.

B XRD diffractograms

The XRD diffractogram were mainly used to calculated the amount of phases present with the program Topas. Because all the results are very similar the results were not presented in the results.

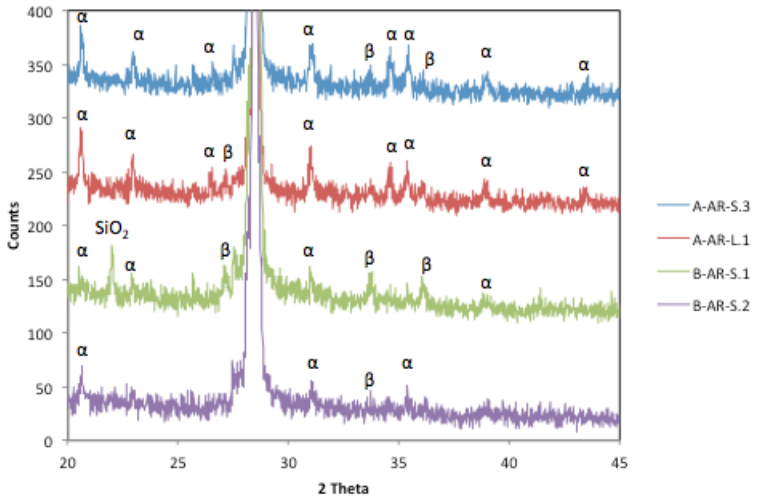

Figure B.1: XRD scans of as received nitrided samples from batch A and B, both TGA nitridations and large scale nitridation.

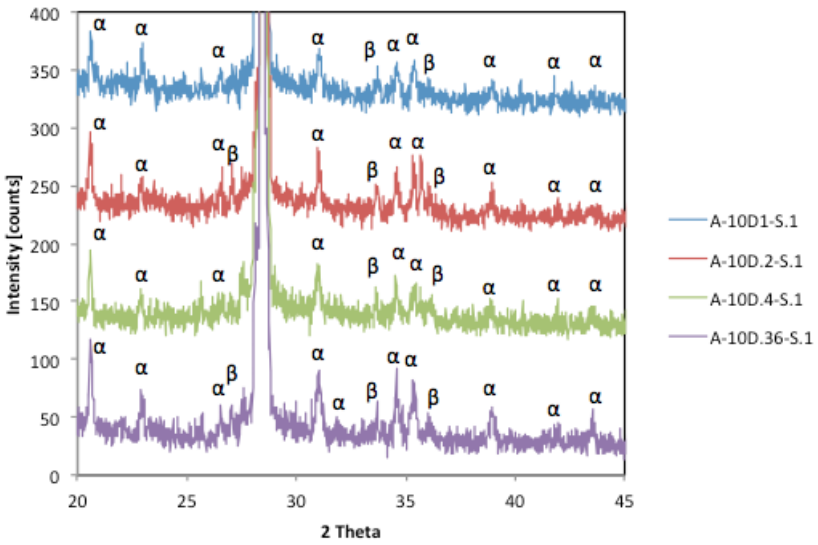

Figure B.2: XRD scans of TGA nitrided samples after different storage times at 10°C.

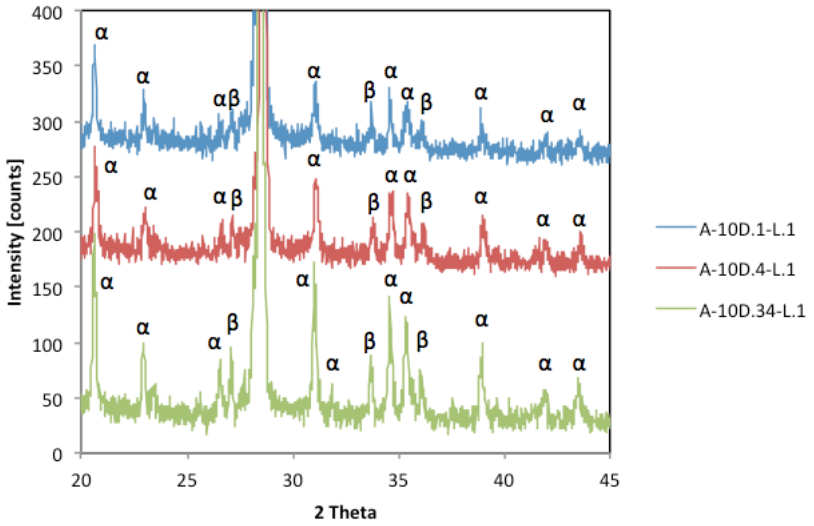

Figure B.3: XRD scans of large scale nitrided samples after different storage times at 10°C.

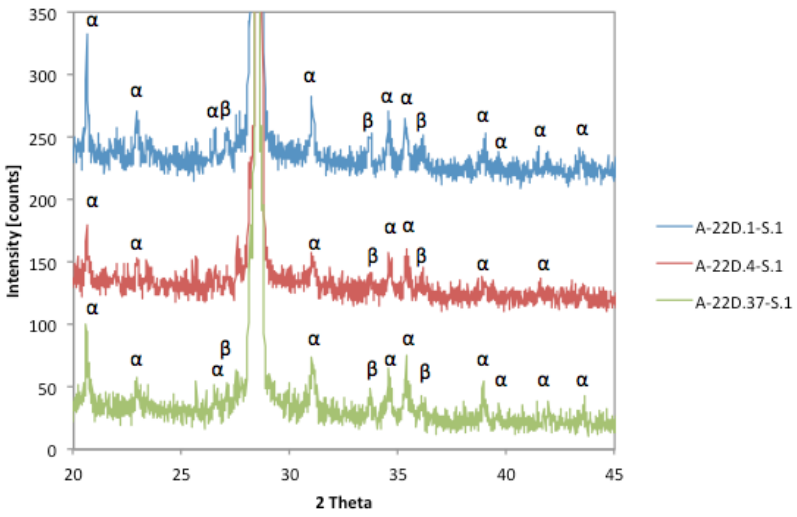

Figure B.4: XRD scans of TGA nitrided samples after different storage times at 22°C

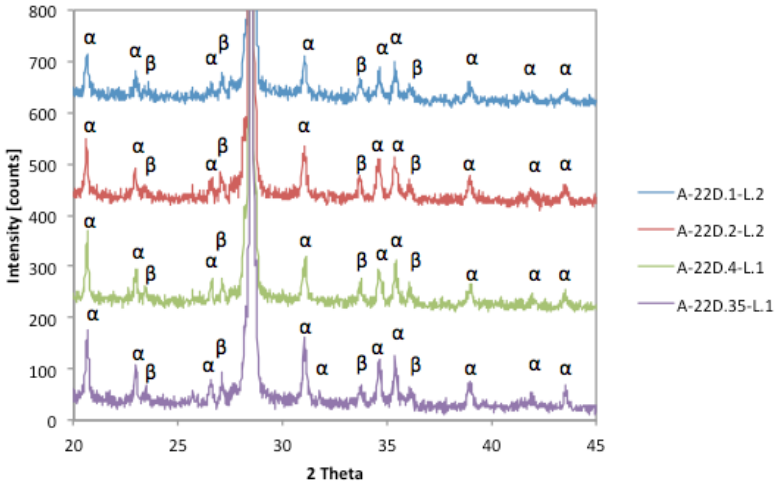

Figure B.5: XRD scans of large scale nitrided samples after different storage times at 22°C

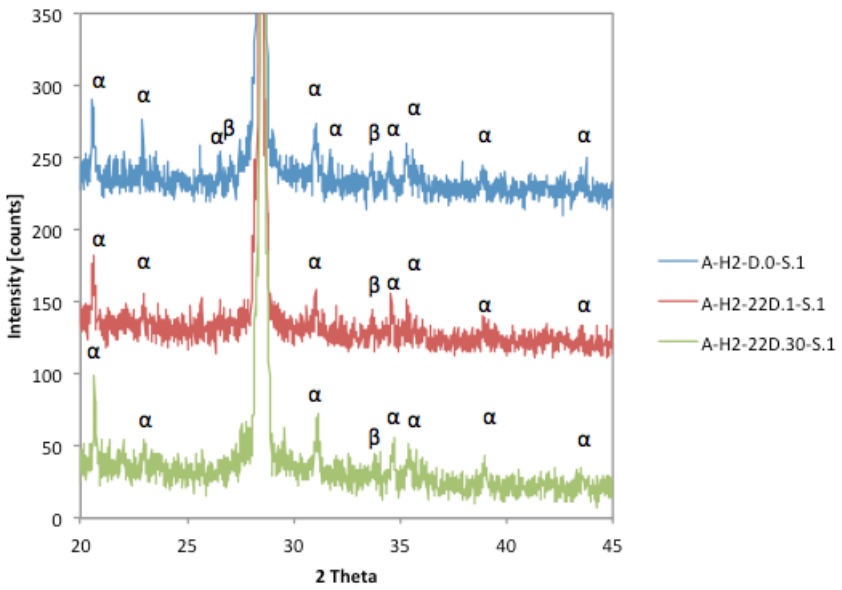

Figure B.6: XRD scans of samples nitrided after being thermally reduced at 1200°C.

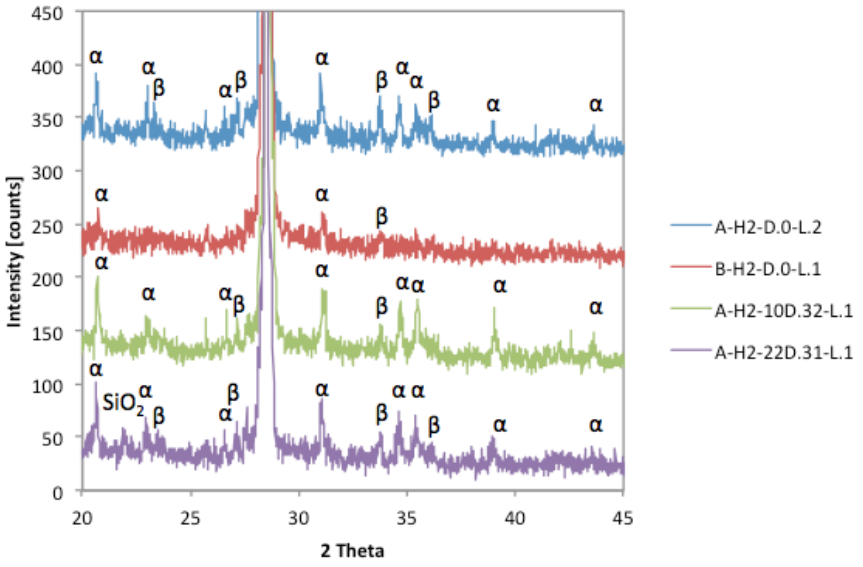

Figure B.7: XRD scans of samples nitrided after being thermally reduced at 1300°C.

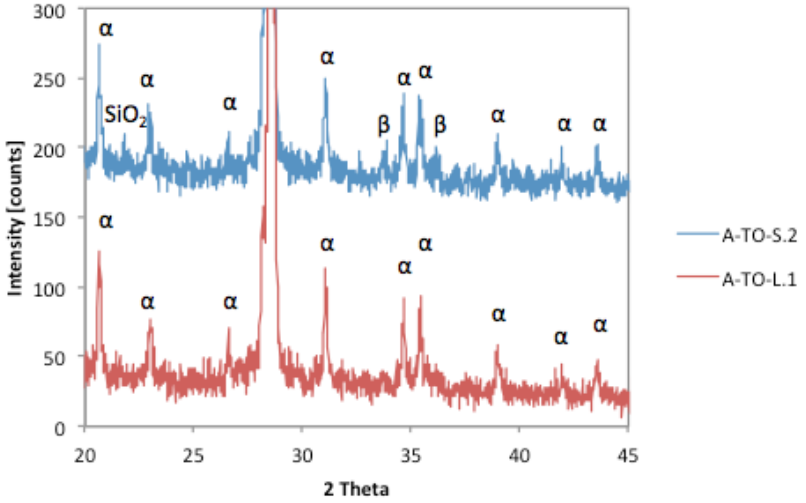

Figure B.8: XRD scans of samples nitrided after a thermal oxidation.

C Data tables for all samples

Table C.1: Amount of α- and β-Si_3N_4. The error in the analysis is given in parenthesis

Sample	*α [%]*	*β [%]*	*Si [%]*	*α/β-ratio*
A-AR-S.3*	10.00 (66)	1.10 (40)	88.90 (75)	0.901
A-AR-L.1	12.45 (75)	2.40 (59)	85.14 (87)	0.838
A-AR-L.2	8.37 (43)	2.56 (33)	89.07 (52)	0.766
B-AR-S.1	0.89 (28)	2.43 (32)	96.68 (42)	0.268
B-AR-S.2*	1.79 (37)	0.49 (25)	97.72 (44)	0.785
A-10D.1-S.1	6.40 (47)	1.43 (32)	92.17 (56)	0.817
A-10D.2-S.1	7.32 (49)	2.21 (33)	90.47 (57)	0.768
A-10D.4-S.1	7.19 (53)	2.61 (52)	90.19 (71)	0.734
A-10D.36-S.1*	11.71 (56)	2.37 (40)	85.92 (66)	0.832
A-10D.1-L.1	11.33 (57)	3.33 (41)	85.34 (68)	0.773
A-10D.4-L.1	16.29 (56)	4.40 (39)	79.31 (65)	0.787
A-10D.35-L.1	18.61 (46)	4.30 (28)	77.09 (52)	0.812
A-22D.1-S.1	8.42 (49)	3.12 (37)	88.46 (59)	0.729
A-22D.4-S.1	5.94 (54)	1.63 (42)	92.43 (67)	0.785
A-22D.36-S.1*	9.01 (56)	1.74 (32)	89.25 (63)	0.838
A-22D.1-L.1	11.21 (44)	4.09 (32)	84.70 (53)	0.733
A-22D.1-L.2	10.88 (63)	3.50 (44)	85.62 (74)	0.757
A-22D.2-L.1	9.57 (41)	2.51 (26)	87.92 (48)	0.792
A-22D.2-L.2	13.11 (40)	3.32 (25)	83.57 (46)	0.798
A-22D.4-L.1	12.38 843)	3.69 (30)	83.93 (51)	0.770
A-22D.34-L.1	14.20 (39)	3.24 (25)	82.56 (46)	0.814
A-H2-D.0-S.1 (1200)	7.41 (55)	1.61 (39)	90.98 (66)	0.821
A-H2-D.0-L.1 (1200)	4.84 (37)	1.19 (24)	93.96 (43)	0.803
A-H2-22D.1-S.1 (1200)	5.52 (44)	1.56 (26)	92.92 (51)	0.780
A-H2-22D.30-S.1 (1200)	6.29 (53)	1.49 (40)	92.21 (65)	0.808
A-H2-22D.30-S.2 (1200)	4.75 (44)	1.18 (26)	94.07 (51)	0.801
A-H2-22D.1-L.1 (1200)	5.06 (38)	1.16 (25)	93.78 (45)	0.813
A-H2-D.0-L.2	5.88 (40)	2.57 (31)	91.55 (49)	0.696
A-H2-D.0-L.3	7.72 (48)	1.67 (36)	90.62 (58)	0.822
B-H2-D.0-S.1	0.22 (26)	0.27 (20)	99.51 (33)	0.449
B-H2-D.0-L.1	1.25 (26)	1.08 (32)	97.67 (41)	0.536
A-H2-10D.1-S.2	4.21 (46)	1.39 (39)	94.40 (60)	0.752
A-H2-10D.32-S.1*	5.99 (56)	1.54 (37)	92.47 (66)	0.795
A-H2-10D.32-L.1	8.49 (44)	2.12 (32)	89.39 (53)	0.800
A-H2-22D.1-S.1	4.77 (51)	0.90 (36)	94.34 (61)	0.841
A-H2-22D.2-S.1	4.98 (50)	1.94 (39)	93.08 (62)	0.720
A-H2-22D.32-S.1*	4.18 (36)	1.72 (30)	94.11 (46)	0.708
A-H2-22D.31-L.1	6.65 (40)	1.90 (29)	91.45 (48)	0.778
A-TO-S.1*	9.19 (59)	1.17 (36)	89.64 (67)	0.887
A-TO-S.2*	14.40 (52)	1.94 (30)	83.66 (58)	0.881
A-TO-L.1	15.32 (58)	1.36 (40)	83.32 (66)	0.918

Table C.2: TGA nitridation of powder from Batch A

Sample code	*Pre-treatment*	*Storage condition*	*Storage time*	*Init. Weight [mg]*	*Weight increase [%]*
A-AR-S.1	None	Dry (exicator)	0	19.29	5.90
A-AR-S.2			0	20.25	4.35
A-AR-S.3*			0	31.32	7.50*
A-10D.1-S.1	None	10°C - humid 0.012 atm.	1	18.76	4.20
A-10D.2-S.1			2	22.84	4.25
A-10D.4-S.1			4	19.63	3.97
A-10D.36-S.1*			36	34.62	6.67*
A-22D.1-S.1	None	22°C - humid	1	21.49	4.70
A-22D.4-S.1			4	17.51	2.97
A-22D.36-S.1*			36	34.61	7.74*
A-H2-D.0-S.1	5%H_2/Ar (1200°C)	None	0	18.24	6.80
A-H2-22D.1-S.1	(1200°C)	22°C-humid 0.026 atm.	1	17.39	6.90
A-H2-22D.30-S.1			30	16.56	5.86
A-H2-22D.30-S.2			30	18.21	3.51
A-H2-10D.1-S.2	5%H_2/Ar (1300°C)	10°C - humid 0.12 atm.	1	32.68	5.08*
A-H2-10D.32-S.1*			32	35.30	4.53*
A-H2-22D.1-S.2	5%H_2/Ar (1300°C)	22°C - humid 0.026 atm.	1	18.89	5.24
A-H2-22D.2-S.1			2	17.12	4.38
A-H2-22D.32-S.1*			32	31.62	5.66*
A-TO-S.1*	Thermal oxidation (900°C)	None	0	44.44	3.58*
A-TO-S.2*			0	36.47	7.98*

Table C.3: Large scale nitridation of powder from Batch A

Sample code	*Pre-treatment*	*Storage condition*	*Days in humid storage*	*Init. Weight [mg]*	*Weight increase [%]*
A-AR-L.1	None	Dry (exicator)	0	359	3.79
A-AR-L.2			0	950.7	3.19
A-10D.1-L.1		10°C-humid	1	293.1	4.84
A-10D.4-L.1	None	0.012 atm.	4	301.6	5.97
A-10D.33-L.1			33	276.2	6.66
A-22D.1-L.1			1	990	4.38
A-22D.1-L.2			1	241.1	5.43
A-22D.2-L.1	None	22°C-humid	2	886.8	3.95
A-22D.2-L.2		0.026 atm.	2	237.8	5.05
A-22D.4-L.1			4	301.1	5.21
A-22D.34-L.1			34	252.2	6.46
A-H2-D.0-L.1	5%H_2/Ar (1200°C)	None	0	832	2.10
A-H2-22D.1-L.1	5%H_2/Ar (1200°C)	22°C - humid	1	846	1.91
A-H2-D.0-L.2	5%H_2/Ar (1300°C)	None	0	257.5	2.14
A-H2-D.0-L.3	5%H_2/Ar (1300°C)		0	222.7	1.71
A-H2-10D.32-L.1	5%H_2/Ar (1300°C)	10°C - humid	32	308.2	2.34
A-H2-22D.31-L.1		22°C - humid	31	191.7	2.87
A-TO-L.1	Thermal oxidation	None	0	353.3	1.13

D Trends in nitridation due to storage time

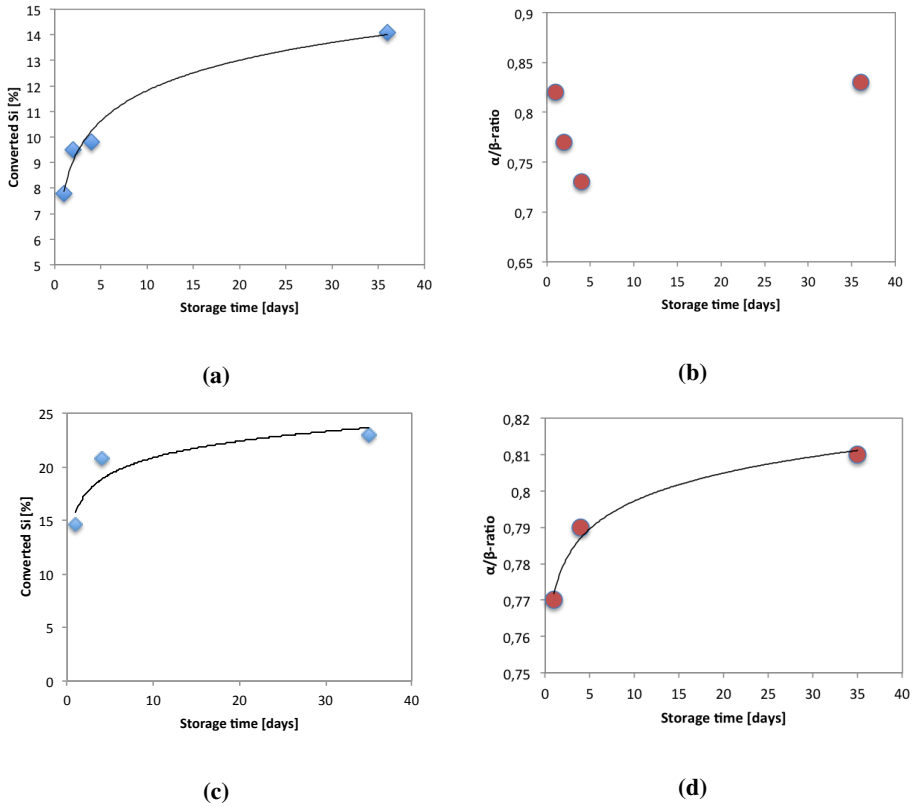

Figure D.1: The figure depicts trends in the TGA (**a**, **b**) and large scale (**c**, **d**) nitrided samples which were stored at 10°C before nitridation. **a**) The conversion of silicon as a function of storage time seems to have a logarithmic trend; **b**) There seems to be no clear trend; **c**) The conversion of silicon as a function of storage time seems to have a logarithmic trend; **d**) The evolution of the α/β-ratio also seem to follow a slightly logarithmic trend.

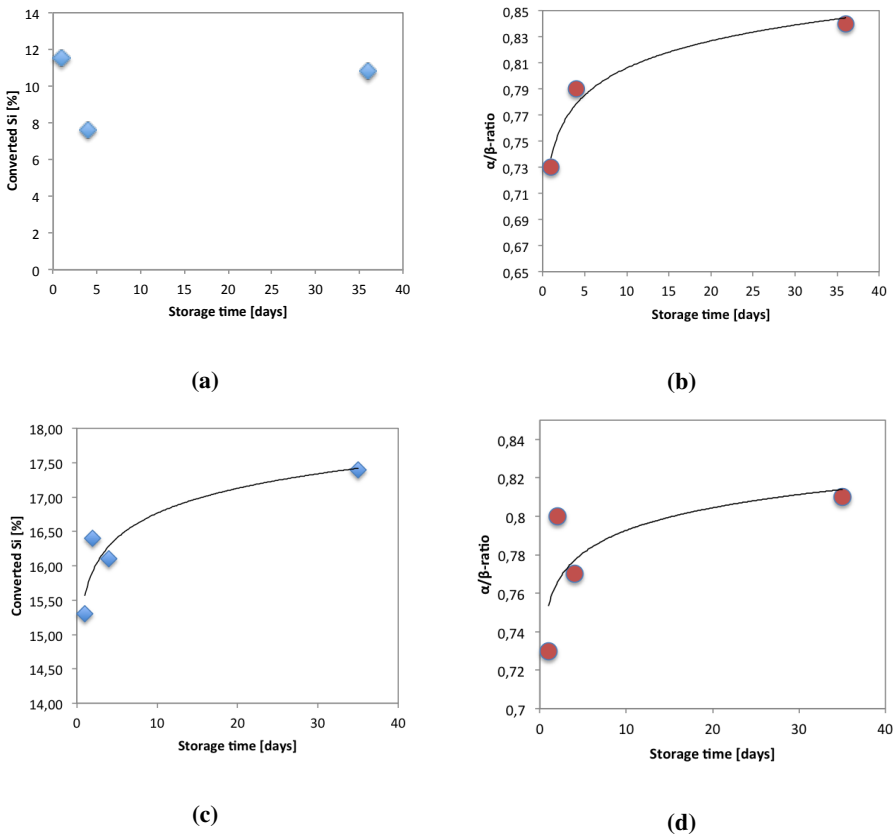

Figure D.2: The figure depicts trends in the TGA (**a**, **b**) and large scale (**c**, **d**) nitrided samples which were stored at 22°C before nitridation. **a**) The conversion of silicon as a function of storage time does not follow a specific trend; **b**) The evolution of the α/β-ratio seem to follow a logarithmic trend; **c**) The conversion of silicon as a function of storage time have a logarithmic trend; **d**) The evolution of the α/β-ratio also follows a logarithmic trend.

E EDS analyses

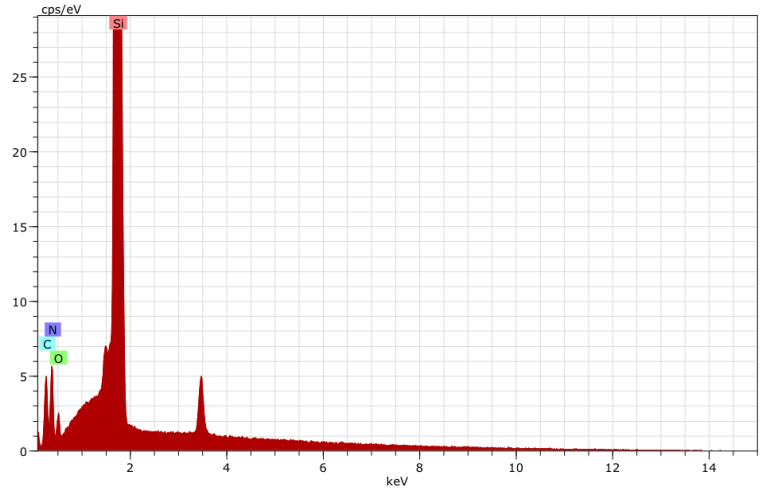

Figure E.1: EDS analysis of sample A-22D.1-S.1

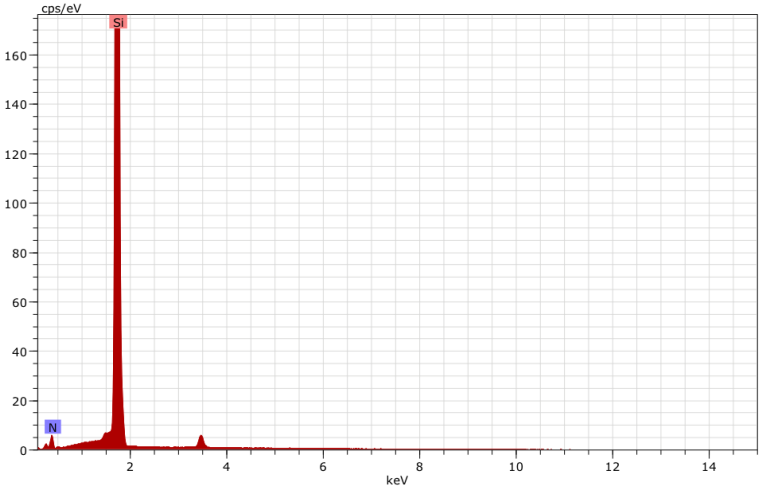

Figure E.2: EDS analysis of sample A-H2-22D.32-S.1

The two figures above show that the thermally reduced sample has no traces of oxygen, in contrast to the sample stored directly at 22°C.

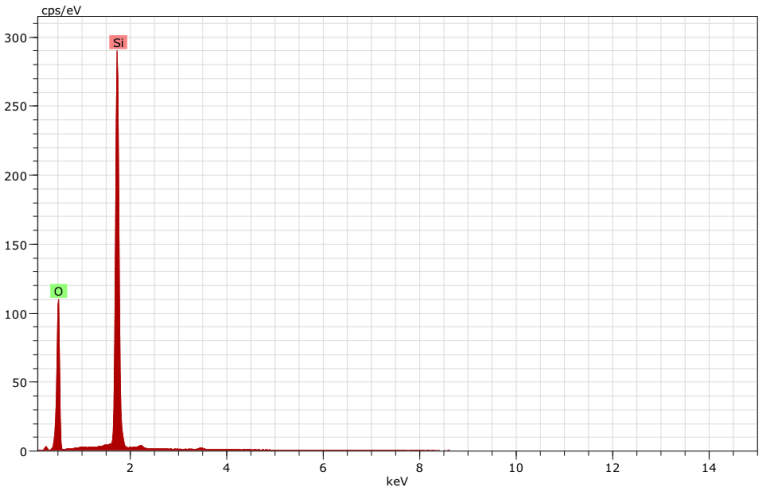

Figure E.3: EDS analysis of the product formed on the crucible wall on sample A-TO-S.2*. The results strongly indicate that the product is SiO_2.

F Comparison of α-Si_3N_4 and SiO_2 whiskers

Both α-Si_3N_4 and SiO_2 can form what is usually called whiskers. As can be seen in figure 4.5.2 these products look very similar. EDS was done on the SiO_2 to confirm the presence of Si and O, but that is harder to do with α-Si_3N_4. The reason is that α-Si_3N_4 whiskers are much smaller and the result from the EDS usually picks up much of the underlying background and therefore gives an incorrect result. The best indication of which is which is therefore a comparison of the sizes. The figure shows that the SiO_2 whiskers are much longer and thicker.

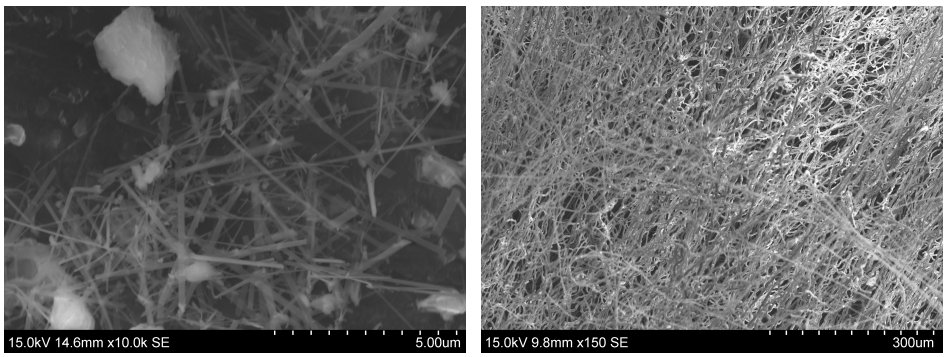

(a) **(b)**

Figure F.1: The figure shows the difference between α-Si_3N_4 (**a**)) and SiO_2 (**b**)) whiskers. The silicon nitride whiskers are much shorter in length, whereas the SiO_2 whiskers can cover several hundred μm.

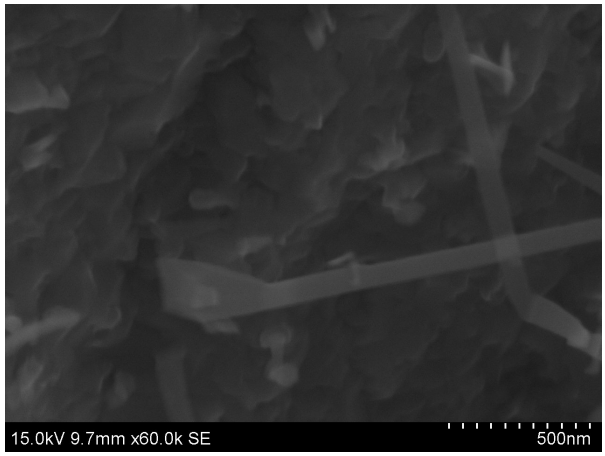

Figure F.2: The figure show the thickness of α-Si_3N_4 whiskers. It can be seen that the whiskers are approximately 100 nm thick.

G Deviations in the TGA curves

Some of the results gained from the TGA nitridation was discarded due to a total mass loss. The first figure below show the TGA curves for these samples. There is a clear reduction in weight very early in the nitridation. These curves have not been fitted in the same way as the ones presented in the results. The x-axis show time only and the area of interest lies at around 30 minutes which corresponds to a temperature of about 300°C.

The second figure shows the TGA curves of two samples that showed a lower weight increase than expected, but were not discarded. Similarities can be seen in the two figures.

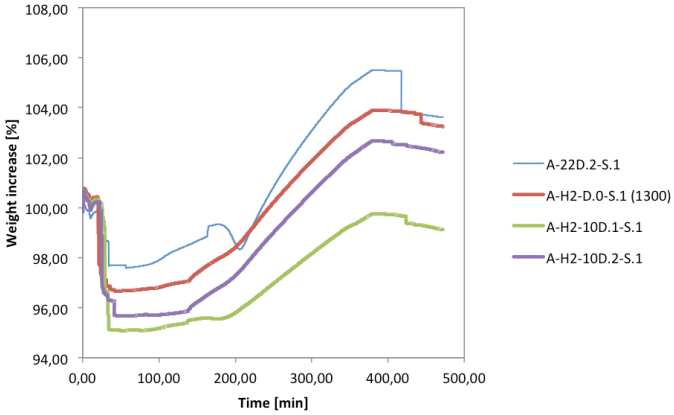

Figure G.1: TGA curves for samples that were discarded.

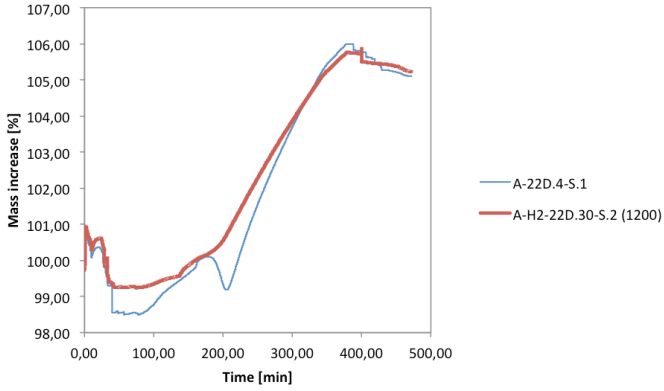

Figure G.2: TGA curves for samples that showed lower weight increase than expected but were not discarded.

H Calculation of SiO_2 thickness

Based on the observed weight reduction from SiO(g) it can be calculated how much SiO_2 is required to produce the corresponding weight loss.

For this calculation it is assumed that the average SiO(g) weight loss is 1% and that the oxide layer is amorphous silica. A sample of 20 mg is also assumed.

Data:
BET surface area, A = 0.8330 m^2/g
SiO_2 density, $\delta = 2.5$ * g/cm^3
$M_{SiO} = 44.08$ g/mol
$M_{SiO_2} = 60.08$ g/mol

First the amount of evaporated SiO(g) is calculated in mols:

$$n_{SiO} = \frac{20\times10^{-3}\times0.01}{44.08} = 4.54 \times 10^{-6} \text{ mol}$$

The mass balance of the active oxidation reaction tells us we need half as many mols of SiO_2 as SiO to complete the reaction. We can now calculate the total weight of SiO_2 needed:

$$m_{SiO_2} = \frac{4.54\times10^{-6}}{2} mol \times 60.08 g/mol = 1.36 \times 10^{-4} \text{ g}$$

The mass of the needed SiO_2 corresponds to the following volume:

$$V_{SiO_2} = \frac{1.36\times10^{-4}}{2.5 g/cm^3 \times 100^3 cm^3/m^3} = 5.44 \times 10^{-11} m^3$$

Calculation of the surface area of a 20 mg sample:

$$20 \times 10^{-3} \text{ g} \times 0.8330 \text{ m}^2/\text{g} = 0.01666 \text{ m}^2$$

The necessary thickness of the oxide layer can now be calculated:

$$SiO_2 \text{ thickness} = \frac{5.44\times10^{-11} m^3}{0.01666 m^2} = 3.27 \text{ nm}$$

*Papirer (2000) reports that the density of amorphous surface silica lies between 2-3 g/cm^3

I Calculation of Si_3N_4 layer thickness

The average, sudden weight increase present in some of the TGA curves was approximately 0.5%. Here, the assumptions and equations for calculating the related Si_3N_4 layer thickness will be presented.

The calculations are based on the assumption that a sample of 20 mg are nitrided and that the Si_3N_4 layer will cover the entire sample surface. In addition it is assumed that the layer has a uniform density.

Data:
BET surface area, A = 0.8330 m^2/g
Si_3N_4 density, δ = 3.1[†] g/cm^3

Calculation of the surface area of a 20 mg sample:

$$20 \times 10^{-3}\ \text{g} \times 0.8330\ \text{m}^2/\text{g} = 0.01666\ \text{m}^2$$

Calculation of the volume that corresponds to 0.5% weight increase:

$$\frac{0.005 \times 20 \times 10^{-3} g}{3.1 \times 100^3 g/m^3} = 3.23 \times 10^{-11}\ \text{m}^3$$

Dividing the sample surface by the increased volume following a 0.5% weight increase gives the Si_3N_4 layer thickness:

$$\frac{3.23 \times 10^{-11} m^3}{0.01666 m^2} = 1.94\ \text{nm}$$

[†] den (Memsnet.org)

J Reaction rates for selected samples

The table presented below shows the slopes of the curves, i.e. the reaction rates from the isothermal segment of the nitridation program. The reaction rates are more or less the same for the samples that only differ in storage time and therefore only one sample from each "parallel" has been calculated.

Table J.1: Reaction rates from the isothermal section.

Sample	*Reaction rate [%]/min*
A-AR-S.3*	0.032
A-10D.1-S.1	0.033
A-22D.1-S.1	0.029
A-H2-D.0-S.1	0.026
A-H2-10D.1-S.1	0.025
A-H2-22D.1-S.1	0.034
A-TO-S.2*	0.036